*J. Fluid Mech.* (1977), *vol.* 83, *part* 4, *pp.* 609–640
*Printed in Great Britain*



# The interaction of sound with a subsonic jet issuing from a semi-infinite cylindrical pipe

By R. M. MUNT
Mathematics Department, University of Dundee, Scotland

(Received 29 June 1976 and in revised form 28 June 1977)

The transmission of sound out of a semi-infinite circular jet pipe in the presence of subsonic flow from the pipe is investigated. An unstable cylindrical vortex layer attached to the edge of the pipe is considered across which differences in mean subsonic flow, density and temperature are included. A solution satisfying the Kutta condition and causality is found which possesses an instability wave term that dominates within a region of approximately 45° to the downstream jet axis. It is shown that when an exterior flow is imposed the noise level increases upstream whilst the instability wave weakens downstream. The stable part of the solution is shown to agree very well with some recent experimental results.

## 1. Introduction

In this paper we shall consider a simple theoretical model for the propagation of sound out of a circular jet pipe in the presence of jet flow. The earliest published work discussing this problem was that of Carrier (1956); however we now believe that he proposed an incorrect boundary condition on the vortex layer which separates the jet flow from the surrounding gas. Subsequent work on the jet-pipe problem has mainly concentrated on the case when the exterior gas flows at the same speed as the jet and is reported by Lansing, Drischler & Pusey (1970), Candel (1973), Munt (1975) and Homicz & Lordi (1975). Recently Savkar (1975) has presented a solution to the problem with mismatch of the flow, extending Mani's (1973) work on the two-dimensional jet to the cylindrical case. Both Mani and Savkar, however, ignore the presence of any instability of the vortex layer in their model. We shall include instabilities in our mathematical treatment of the problem. Lee & Jones (1973) have also included instabilities but their solution does not satisfy the boundary conditions on the exterior of the pipe.

Instabilities have particular theoretical significance for diffraction problems involving a surface edge shedding an unstable shear layer. This has been clearly demonstrated by Morgan (1974) and Crighton & Leppington (1974) in their analysis of a two-dimensional problem involving the interaction of an acoustic source with a semi-infinite vortex sheet which is shed from a rigid splitter plate. They independently show that an instability in the vortex sheet is triggered by the incident acoustic disturbance and in the acoustic field gives rise to a large amplitude wave (the instability wave) effective downstream within a wedge at 45° to the vortex sheet. The solution is unlike that for the infinite vortex sheet (Jones & Morgan 1972), where if one ignores the instability wave the acoustic field outside the wedge remains unaltered. For when the vortex sheet is coupled to a rigid splitter plate one cannot ignore instabilities without

disrupting the remainder of the acoustic field. This is because the stable portion of the field alone does not satisfy all the boundary conditions. A similar situation arises when Morgan's (1975) work on the stability of the cylindrical jet is extended to include a jet nozzle.

Several authors have discussed the spatial instability modes of a cylindrical jet in the absence of acoustic sources. Batchelor & Gill (1962) determined these modes from n eigenequation which is a special case of the equation we discuss in § 3. Some observed directional sound waves that radiated from a supersonic jet have been explained by Tam (1971) in terms of an instability in the vortex layer but he restricted himself to high frequencies. Similar work has been pursued by Crow & Champagne (1971) and Chan & Westley (1973). The former authors and Lee & Jones (1973) find additional solutions to their eigenequation in some special circumstances but cannot reject these other than by physical conjecture. We shall show that these additional solutions are part of a system of zeros of the eigenequation and that, when acoustic sources are present, this system has no influence upon the stability of the field. These results are an extension of some qualitative details that have been rigorously examined by Morgan (1975).

Whether instabilities are relevant or not for a real turbulent jet is, however, a subject of some controversy. In our thin-shear-layer model the instability wave is predicted downstream of the jet nozzle within a cone whose generator makes an angle of around 40°–45° with the jet axis. Indeed a large amplification in this region was found experimentally by Crow (1972) for a high speed jet. On the other hand Savkar (1975) suggests, by reference to unpublished experiments, that only for jet Mach numbers in excess of 0·7 does the instability wave appear. Pinker & Bryce (1976), however, in their careful experimental measurements, taken at angles down to 35°, do not observe an instability wave for a cold jet even for a jet Mach number as high as 0·95. The controversy might be mathematically resolved by allowing for the thickness of the shear layer. For instance Jones (1977) has shown that for an infinite plane shear layer there is a critical Strouhal number, based on the shear-layer thickness, above which the instability wave does not exist. Further, when the instability does exist, the angle of influence is dependent on the Strouhal number and decreases to zero as the Strouhal number approaches the critical value. Similar results may be expected to apply in the cylindrical case; however such a study is beyond the scope of the present paper.

Another topic of some uncertainty is that of the correct condition to apply at the trailing edge of a pipe or plane. Orszag & Crow (1970) were the first to consider the edge conditions for an unstable shear layer coupled to a semi-infinite flat plate. In their analysis, which excluded sound sources and was for incompressible flow, they suggested that one of three possible conditions may apply at the trailing edge: namely (i) the 'full Kutta condition', (ii) a 'rectified Kutta condition' or (iii) no Kutta condition. Their analysis was extended by Crighton (1972*a*, *b*) to include compressibility. Neither Crighton nor Orszag & Crow prove conclusively which edge condition should apply.

For the problem incorporating a sound source Morgan (1974) and Crighton & Leppington find that there is an infinity of causal solutions, only one of which satisfies the 'full Kutta condition' that the edge velocity be finite, the remainder giving infinite velocities at the edge. They favour the unique solution satisfying the 'full Kutta condition'. Indeed Bechert & Pfizenmaier (1975) have provided experimental evidence

to suggest that the 'full Kutta condition' is the correct condition to apply if the shear layer is thin, which is certainly the case in the model used by Morgan and Crighton & Leppington. Therefore, since we have also assumed a thin shear layer, we shall adopt the 'full Kutta condition' at the nozzle of the jet pipe. However we should mention that, for a shear layer of finite thickness, Bechert & Pfizenmaier have observed a dependence of the exit condition on the Strouhal number based on the shear-layer thickness. For high Strouhal numbers they suggest that the 'no Kutta (or parabolic) condition' of Orszag & Crow is appropriate. Difficulties of uniqueness arise if we attempt to relax the Kutta condition so we shall not pursue such an analysis here, although Howe (1976) has found that at very low Mach numbers the effect of relaxing the Kutta condition is to increase the radiated sound level.

In the following section the mathematical model is established with the acoustic disturbances having harmonic time dependence $\exp(i\omega t)$. For analytical convenience we allow for complex values of the wavenumber $k = \omega/c_j$, where $c_j$ is the speed of sound in the jet. A formal solution is then obtained for $k$ lying within a special region in the lower half $k$ plane. The contour bounding this region is determined by certain zeros of an eigenequation whose properties we analyse in § 3. Ultimately we are interested in the solution for real $k$ and to retain regularity in the $k$ plane it is necessary to eliminate a singularity which occurs in the solution on the aforementioned contour.

Section 4 deals with the splitting of the eigenequation. This is necessary for the application of the Wiener–Hopf procedure followed here. Other authors have used approximations to evaluate similar split functions. Crighton (1972*b*), for instance, considered the limits of high and low frequency whilst Savkar (1975) used the Carrier–Koiter approximation.

In § 5 we consider the question of causality. This is usually investigated by analysing the initial-value problem and demanding that the acoustic field is zero before the source is triggered. The significance of pursuing such an analysis has been established by Jones & Morgan (1972). Hardisty (1975) has used similar ideas for the treatment of the instability of a two-dimensional jet under acoustic radiation. On the other hand Morgan (1975), in his analysis of the cylindrical vortex layer, answers the causality question by applying a theorem of Jones & Morgan (1974). The validity of this theorem has been demonstrated by Morgan (1974) in dealing with the semi-infinite vortex sheet and we shall examine causality in the same way.

The acoustic far field is evaluated in § 6 and contains the instability term arising from causality. In § 7 we compare the computed far field with the results of (i) Savkar's (1975) theory, (ii) the experiments of Plumblee & Dean (1973) and (iii) the experiments of Pinker & Bryce (1976). Agreement with the latter work is particularly good for a cold jet operating in static and flight (simulated) conditions.

## 2. Formulation of the problem

The problem we consider is that of acoustic diffraction by a sound wave propagating out of a rigid semi-infinite cylindrical shell from which also issues a cylindrical jet of fluid, the whole being immersed in a fluid moving axially. The cylinder is specified by $r = a$, $z \leqslant 0$ in cylindrical polar co-ordinates $(r, \Theta, z)$ and the vortex layer, separating the two fluids in relative motion, is taken as the semi-infinite extension of the cylinder

into the region $r = a, z > 0$. Differences between the two fluids in mean values of the density and speed of sound are also included. Viscosity, thermal conductivity and all nonlinearities will be ignored.

The cylindrical jet is taken to have density $\rho_j$, speed of sound $c_j$ and velocity $Mc_j$, directed along the $+z$ axis. Outside the jet the fluid is taken to have density $\gamma\rho_j$, speed of sound $c_j/C$ and velocity $M\alpha c_j$, directed in the same sense as the jet and with

$$0 \leqslant \alpha < 1.$$

Here the non-dimensional quantities $\alpha, \gamma$ and $C$ express the ratios of the mainstream value to the jet value for the velocity, density and the reciprocal of the speed of sound respectively. The sound source is assumed to have harmonic time dependence $\exp(i\omega t)$, this factor being suppressed throughout. Then the equations satisfied by the velocity potential $\phi(r, \Theta, z)$ are

$$\frac{\partial^2\phi}{\partial z^2} + \frac{1}{r}\frac{\partial}{\partial r}\left(r\frac{\partial\phi}{\partial r}\right) + \frac{1}{r^2}\frac{\partial^2\phi}{\partial\Theta^2} - \left(ik + M\frac{\partial}{\partial z}\right)^2\phi = 0, \quad r < a, \tag{2.1}$$

$$\frac{\partial^2\phi}{\partial z^2} + \frac{1}{r}\frac{\partial}{\partial r}\left(r\frac{\partial\phi}{\partial r}\right) + \frac{1}{r^2}\frac{\partial^2\phi}{\partial\Theta^2} - C^2\left(ik + M\alpha\frac{\partial}{\partial z}\right)^2\phi = 0, \quad r > a, \tag{2.2}$$

where $k = \omega/c_j$.

From the assumption that the cylinder is perfectly rigid, reflecting all sound, one derives the boundary condition that the normal derivative of $\phi$ vanishes on the cylinder, viz.

$$\partial\phi(a, \Theta, z)/\partial r = 0, \quad z \leqslant 0. \tag{2.3}$$

The boundary conditions on the vortex layer are the continuity of pressure, so that

$$(ik + M\partial/\partial z)\,\phi(a^-, \Theta, z) = \gamma(ik + M\alpha\partial/\partial z)\,\phi(a^+, \Theta, z), \quad z > 0, \tag{2.4}$$

and the kinematic condition for equal particle displacement on both sides of the vortex layer. Let $\eta(z, \Theta)$ denote the displacement of the vortex layer from its mean position $r = a$; then the latter condition implies that $\eta$ satisfies

$$\left.\begin{aligned} c_j(ik + M\alpha\partial/\partial z)\,\eta(z, \Theta) &= \partial\phi(a^+, \Theta, z)/\partial r, \\ c_j(ik + M\partial/\partial z)\,\eta(z, \Theta) &= \partial\phi(a^-, \Theta, z)/\partial r, \end{aligned}\right\} \quad z > 0. \tag{2.5}$$

At the edge of the cylinder we impose the Kutta condition that the vortex layer should leave the cylinder with zero gradient. We also require that the field be radiating outwards at infinity.

We split the total field $\phi$ into the contributions from the primary wave ($\phi_0$) and the diffracted field ($U$), so that

$$\phi(r, \Theta, z) = \phi_0(r, \Theta, z) + U(r, \Theta, z). \tag{2.6}$$

For the primary wave we have taken

$$\phi_0(r, \Theta, z) = \left\{\begin{aligned} &\frac{J_n(ra^{-1}j'_{n,m})}{2\pi J_n(j'_{n,m})}\exp\{-i(\mu z - n\Theta)\}, \quad r < a, \\ &0, \quad r > a, \end{aligned}\right\} \tag{2.7}$$

which satisfies (2.1) and (2.3) provided that

$$\mu = \{[k^2-(1-M^2)j'^2_{n,m}/a^2]^{\frac{1}{2}} - kM\}/(1-M^2) \tag{2.8}$$

for $ka > j'_{n,m}$. Here $j'_{n,m}$ is the $m$th zero of $dJ_n(y)/dy$ and $J_n(y)$ is the Bessel function of order $n$. Here and elsewhere we have used the notation of Watson (1966) for the Bessel functions. The choice of $\mu$, with $ka > j'_{n,m}$, ensures that the wave is outgoing and for real $k$ does not decay as $z \to \infty$.

A consequence of the form chosen for the primary wave is that the diffracted field has the same $\Theta$ dependence; we write

$$U(r,\Theta,z) = \psi(r,z)\,e^{in\Theta}, \quad \eta(r,\Theta) = h(z)\,e^{in\Theta}. \tag{2.9}$$

To assist the analysis we assume that $k$ has a negative imaginary part. This assumption corresponds to an absorption of sound so we may anticipate that any waves produced will decay at infinity. In particular we define $k = k_r - ik_i = |k|\exp(-i\delta)$, where $0 < \delta < \pi$. At the end of the analysis we shall put $\delta = 0$.

Define the transform $\beta(r, s)$, in terms of its half-range components, by

$$\beta(r,s) = \beta_+(r,s) + \beta_-(r,s),$$

where
$$\beta_+(r,s) = \int_0^\infty \psi(r,z)\,e^{-sz}\,dz, \quad \beta_-(r,s) = \int_{-\infty}^0 \psi(r,z)\,e^{-sz}\,dz \tag{2.10}$$

and $s$ is complex. Then from (2.1) and (2.2) the equations to be satisfied by $\beta$ are

$$\left.\begin{aligned} \frac{1}{r}\frac{\partial}{\partial r}\left(r\frac{\partial\beta}{\partial r}\right) + \left(\lambda_1^2 - \frac{n^2}{r^2}\right)\beta = 0, \quad r < a, \\ \frac{1}{r}\frac{\partial}{\partial r}\left(r\frac{\partial\beta}{\partial r}\right) + \left(\lambda_2^2 - \frac{n^2}{r^2}\right)\beta = 0, \quad r > a, \end{aligned}\right\} \tag{2.11}$$

where $\lambda_1^2 = s^2 - (ik + Ms)^2$ and $\lambda_2^2 = s^2 - C^2(ik + \alpha Ms)^2$. We define $\lambda_1$ to be that branch which reduces to $k$ when $s = 0$. Similarly $\lambda_2$ is defined to be $Ck$ at $s = 0$. The branch cuts for $\lambda_1$ are taken on the line $\arg s = \frac{1}{2}\pi - \delta$ from $ik/(1-M)$ to $i\infty\exp(-i\delta)$ and from $-i\infty\exp(-i\delta)$ to $-ik/(1+M)$. Those for $\lambda_2$ are taken from $iCk/(1-M\alpha C)$ to $i\infty\exp(-i\delta)$ and from $-i\infty\exp(-i\delta)$ to $-iCk/(1+M\alpha C)$.

From now on we shall assume that the jet is subsonic, i.e. $M < 1$. Then it is easily shown that $\lambda_1$ and $\lambda_2$ have negative imaginary parts in the respective strips

$$\frac{-k_i}{1+M} < \operatorname{Re} s < \frac{k_i}{1-M}, \quad \frac{-Ck_i}{1+M\alpha C} < \operatorname{Re} s < \frac{Ck_i}{1-M\alpha C}.$$

Let the strip common to both of these intervals be denoted by

$$-\sigma_1 k_i < \operatorname{Re} s < \sigma_2 k_i. \tag{2.12}$$

We assume that $\psi(r, z)$ is sufficiently well behaved for $\beta(r, s)$ to exist in the strip (2.12); $\beta_+$ exists for $\operatorname{Re} s > -\sigma_1 k_i$ and $\beta_-$ exists for $\operatorname{Re} s < \sigma_2 k_i$. Specifically, since

$$\operatorname{Im}\mu \leqslant -k_i/(1+M)$$

one deduces that the transform $\beta_+$ of the primary wave exists in the strip (2.12).

The solutions to (2.11) are Bessel functions of order $n$. We require the solution which remains finite at $r = 0$, complies with the radiation condition and, when $s$ lies in (2.12), decays as $r \to \infty$. Hence

$$\beta(r,s) = \begin{cases} A(s)\,J_n(\lambda_1 r), & r < a, \\ B(s)\,H_n^{(2)}(\lambda_2 r), & r > a. \end{cases} \tag{2.13}$$

For convenience we introduce two further transformations

$$G(s) = \int_{-\infty}^{\infty} \left[\gamma\left(ik + M\alpha\frac{\partial}{\partial z}\right)\psi(a^+, z) - \left(ik + M\frac{\partial}{\partial z}\right)\psi(a^-, z)\right]\exp(-sz)\,dz \quad (2.14)$$

and

$$F_+(s) = \int_0^{\infty} h(z)\exp(-sz)\,dz. \quad (2.15)$$

Then on applying these to the boundary conditions (2.3)–(2.5) together with equations (2.6), (2.7), (2.9) and (2.13) we obtain

$$G_-(s) = \gamma(ik + M\alpha s)\,B(s)\,H_n^{(2)}(\lambda_2 a) - (ik + Ms)\,A(s)\,J_n(\lambda_1 a) - G_+(s), \quad (2.16)$$

where

$$A(s) = \frac{c_j F_+(s)\,(ik + Ms)}{\lambda_1 J_n'(\lambda_1 a)}, \quad B(s) = \frac{c_j F_+(s)\,(ik + M\alpha s)}{\lambda_2 H_n'^{(2)}(\lambda_2 a)}$$

and

$$G_+(s) = \frac{i(k - \mu M)}{2\pi(s + i\mu)}.$$

Here we have used the notation $J_n'(x) = dJ_n(x)/dx$ and $H_n'^{(2)}(x) = dH_n^{(2)}(x)/dx$. Eliminating $A(s)$, $B(s)$ and $G_+(s)$ from (2.16) then leads to

$$G_-(s) + \frac{i(k - \mu M)}{2\pi(s + i\mu)} = -c_j\frac{F_+(s)\,k^3\chi(s)}{\lambda_1\lambda_2}, \quad (2.17)$$

where

$$\chi(s) = (ik + Ms)^2\frac{\lambda_2 J_n(\lambda_1 a)}{k^3 J_n'(\lambda_1 a)} - \frac{\gamma(ik + M\alpha s)^2\lambda_1 H_n^{(2)}(\lambda_2 a)}{k^3 H_n'^{(2)}(\lambda_2 a)}.$$

We shall solve (2.17) using the Wiener–Hopf technique described, for instance, in Noble's book (1958, chap. 2). To make progress we require some estimate of the behaviour of the functions $F_+(s)$ and $G_-(s)$. First, on the vortex layer and near to the edge of the cylinder we shall apply the full Kutta condition $h(z) = O(z^{\frac{1}{2}})$ as $z \to 0^+$, which implies that $F_+(s) = O(s^{-\frac{3}{2}})$ as $|s| \to \infty$ in the positive half-plane. A second requirement is that the sound pressure should be bounded on the cylinder. So to account for this we assume that $G_-(s) = O(s^q)$ as $|s| \to \infty$ in the negative half-plane; where $q < -1$. Lastly we observe that in a linear model, such as this, the vortex layer has an inherent instability which grows as it propagates downstream. Associated with this instability is the zero $s_0$ of $\chi(s)$, which for positive real $k$ lies in the region $\mathrm{Re}\,s_0 > 0$, $\mathrm{Im}\,s_0 < 0$. The reasons for making the dependence on $s_0$ explicit will become apparent when we deal with causality.

In the usual manner we introduce split functions $\chi_+(s)$ and $\chi_-(s)$, regular in the respective half-planes $\mathrm{Re}\,s > s_1$ and $\mathrm{Re}\,s < s_2$, such that $\chi(s) = \chi_+(s)/\chi_-(s)$. Here, for analytical convenience, $s_1$ and $s_2$ are real numbers which define a narrow strip within (2.12) such that $-\sigma_1 k_i < s_1 < 0 < s_2 < \sigma_2 k_i$. The properties and evaluation of the split functions are discussed in §4 for $\delta \to 0$. It can be deduced that $\chi_-(s)$ has a simple pole at $s_0$ when $k \notin \Delta_0$ and $0 < \delta < \frac{1}{2}\pi$, where $\Delta_0$ is defined in §3. Then the properties

$$\chi_+(s) = O(s^{\frac{3}{2}}), \quad \chi_-(s) = O(s^{-\frac{3}{2}}) \quad (2.18)$$

prevail as $|s| \to \infty$ in appropriate half-planes. However if $k \in \Delta_0$ then $s_0$ lies in the region $\mathrm{Re}\,s < s_1$ and therefore becomes a zero of $\chi_+(s)$. Then

$$\chi_+(s) = O(s^{\frac{5}{2}}), \quad \chi_-(s) = O(s^{-\frac{1}{2}}) \quad (2.19)$$

as $|s| \to \infty$ in the relevant half-planes. This situation occurs when $\alpha = C = \gamma = 1$, for which the region $\Delta_0$ occupies the whole of the lower half $k$ plane. This case is discussed elsewhere (see for instance Munt 1975), so for the remainder of this section we shall restrict considerations to $\alpha < 1$.

When $k \in \Delta_0$ we can rearrange (2.17) to form an equation with one side regular in $\mathrm{Re}\, s < s_2$ and the other side regular in $\mathrm{Re}\, s > s_1$. Thus

$$\frac{i(k-\mu M)}{2\pi(s+i\mu)}\{\chi_-(s)\,\lambda_1^-(s)\,\lambda_2^-(s) - \chi_-(-i\mu)\,\lambda_1^-(-i\mu)\,\lambda_2^-(-i\mu)\} + G_-(s)\,\lambda_1^-(s)\,\lambda_2^-(s)\,\chi_-(s)$$
$$= \frac{-c_j k^3 F_+(s)\,\chi_+(s)}{\lambda_1^+(s)\,\lambda_2^+(s)} - \frac{i(k-\mu M)\,\chi_-(-i\mu)\,\lambda_1^-(-i\mu)\,\lambda_2^-(-i\mu)}{2\pi(s+i\mu)}, \quad (2.20)$$

where $\lambda_1^{\pm}(s) = \{s(1 \pm M) \pm ik\}^{\frac{1}{2}}$, $\lambda_2^{\pm}(s) = \{s(1 \pm M\alpha C) \pm ikC\}^{\frac{1}{2}}$.

In their common strip, $s_1 < \mathrm{Re}\, s < s_2$, the two sides of (2.20) are equal and therefore may be considered as analytic continuations of each other. By a straightforward application of Liouville's theorem, with the estimates discussed earlier, one deduces that the integral function defined by (2.20) is identically zero. Hence

$$F_+(s) = \frac{-i(k-\mu M)\,\chi_-(-i\mu)\,\lambda_1^-(-i\mu)\,\lambda_2^-(-i\mu)\,\lambda_1^+(s)\,\lambda_2^+(s)}{2\pi c_j k^3 \chi_+(s)\,(s+i\mu)}. \quad (2.21)$$

We may now formally recover the diffracted field $U(r, \Theta, z)$ by inverting the transform. Of particular interest is the external field in $r > a$, for which $\psi(r, z)$ is given by

$$\psi(r,z) = \frac{1}{2\pi i}\int_{d-i\infty}^{d+i\infty} \frac{c_j(ik + M\alpha s)\,F_+(s)\,H_n^{(2)}(\lambda_2 r)}{\lambda_2 H_n'^{(2)}(\lambda_2 a)} \exp(sz)\,ds, \quad (2.22)$$

where $s_1 < d < s_2$ and $k \in \Delta_0$. When $k \notin \Delta_0$ and $0 < \delta < \frac{1}{2}\pi$ there is a singularity in $F_+(s)$ at $s_0$ and this implies that the boundary condition (2.3) is not satisfied. However this will be rectified when we deal with the causal solution in § 5.

## 3. The zeros of $\chi$

This section is devoted to locating the zeros of $\chi(s)$. The qualitative details of the location of these zeros for the case $\alpha = 0$ and $C = \gamma = 1$ can be found in a paper by Morgan (1975). Here we shall be concerned with the extension of these results to general values of $\alpha$, $\gamma$ and $C$ and where this is not possible we shall present numerical details.

For convenience we make the transformation $s = -iku$ and replace $\lambda_1$ and $\lambda_2$ by $kv$ and $kw$, respectively, so that

$$\left.\begin{aligned} v^2(u) &= (1-Mu)^2 - u^2 \\ \text{and} \qquad w^2(u) &= C^2(1-M\alpha u)^2 - u^2. \end{aligned}\right\} \quad (3.1)$$

Then
$$\chi(-iku) = \frac{\gamma(1-M\alpha u)^2 v H_n^{(2)}(kaw)}{H_n'^{(2)}(kaw)} - \frac{(1-Mu)^2 w J_n(kav)}{J_n'(kav)}. \quad (3.2)$$

We have chosen the branch cuts for $v$ to be on the real $u$ axis from $1/(1+M)$ to $\infty$ and from $-1/(1-M)$ to $-\infty$. Those of $w$ are taken from $C/(1+M\alpha C)$ to $\infty$ and from $-C/(1-M\alpha C)$ to $-\infty$. At $u = 0$ the function $v$ is unity and $w$ is $C$. Since it is easier to deal with the case when the inequalities (*a*) $-C/(1-M\alpha C) < -1/(1-M)$ and (*b*)

$1/(1+M) < C/(1+M\alpha C)$ hold simultaneously we shall, for most of the discussion, assume that this case prevails; since $0 < M < 1$ and $0 < \alpha < 1$, this implies that $C > 1/[1-M(1-\alpha)] > 1$. Where appropriate we shall indicate the differences that occur when $(a)$ or $(b)$ does not hold. These alternatives will be referred to as follows.

$$\text{Case I: } -1/(1-M) < -C/(1-M\alpha C).$$

$$\text{Case II: } C/(1+M\alpha C) < 1/(1+M).$$

The former case (I) can occur with $(b)$ or its converse case II but case II can exist only with case I. The combination of case I with $(b)$ is the one that occurs when the acoustic speeds of the two media are the same; i.e. for a cold jet with $C = 1$.

We shall first discuss the approximation to the zeros of (3.2) for positive real $k$ in the limits of very high and very low frequencies. Later in this section we shall describe some numerical details for real and complex $k$.

In the high frequency limit, when $ka \gg 1$, we can expand the Bessel functions asymptotically, provided that $u$ is not within a distance of $(ka)^{-2}$ from the branch points. Then

$$\chi(-iku) \sim i\gamma(1-M\alpha u)^2 v + (1-Mu)^2 w \cot(kav - \tfrac{1}{2}n\pi - \tfrac{1}{4}\pi). \tag{3.3}$$

Where $\operatorname{Im} v < 0$ the zeros of (3.3) are of the order of $\exp(2ka \operatorname{Im} v)$ from those of

$$\gamma v(1-M\alpha u)^2 + (1-Mu)^2 w = 0 \tag{3.4}$$

and in the region $\operatorname{Im} v > 0$ the zeros are of the order of $\exp[-2ka \operatorname{Im} v]$ from those of

$$\gamma v(1-M\alpha u)^2 - (1-Mu)^2 w = 0. \tag{3.5}$$

If we further assume that $\gamma = C^2$, i.e. $\rho c^2$ is a constant across the vortex layer, then we may write (3.4) and (3.5) as

$$(v+w)(wv+u^2) = 0 \tag{3.6}$$

and

$$(v-w)(wv-u^2) = 0 \tag{3.7}$$

respectively. There are two zeros of $v-w=0$, namely

$$u_4 = \frac{1-C}{M(1-\alpha C)}, \quad u_5 = \frac{1+C}{M(1+\alpha C)};$$

$v+w=0$ has no zeros. To determine the remaining zeros explicitly it is necessary to consider the case $C=1$; i.e. case I occurs. Then the zeros of $wv+u^2=0$ are

$$u_0, u_1 = \frac{2\xi}{M}\left\{\frac{\xi(1+\alpha) \pm i\eta(1-\alpha)}{\xi^2(1+\alpha)^2 + \eta^2(1-\alpha)^2}\right\} \tag{3.8}$$

and the zeros of $wv-u^2=0$ are

$$u_2, u_3 = \frac{2\xi'}{M[\xi'(1+\alpha) \pm \eta'(1-\alpha)]},$$

where the plus signs go with $u_0$ and $u_2$,

$$\left.\begin{aligned} \xi &= \{1+[M^2(1-\alpha)^2+1]^{\frac{1}{2}}\}/M(1-\alpha), \\ \eta &= \{2\xi/M(1-\alpha)-1\}^{\frac{1}{2}}, \\ \xi' &= \{-1+[M^2(1-\alpha)^2+1]^{\frac{1}{2}}\}/M(1-\alpha) \end{aligned}\right\} \tag{3.9}$$

and

$$\eta' = \{2\xi'/M(1-\alpha)+1\}^{\frac{1}{2}}.$$

Let us now consider which of the zeros $u_i$ are close to actual zeros of (3.2). The zero $u_0$ lies in the region $\operatorname{Im} v < 0$ but $u_1$ violates this condition and so, of these two, only $u_0$ can be close to a zero of (3.2). For $u_2$ and $u_3$ it is easily shown that, as they lie on the real line between the branch cuts, the condition on $\operatorname{Im} v$ is violated. Hence neither can be a zero of $\chi$. The remaining two zeros, $u_4$ and $u_5$, need closer investigation. First consider $u_5$. This lies on the branch cut to the right of the branch points $1/(1+M)$ and $C/(1+M\alpha C)$. To decide on which side of the cut the zero lies a better approximation to $u_5$ can be derived by first noting that (3.2) can be rearranged in the case $\gamma = C^2$ to give

$$\chi(-iku) = -\frac{wJ_n(kav)}{J_n'(kav)}\left\{\left[u-\frac{1+C}{M(1+\alpha C)}\right]\left[u-\frac{1-C}{M(1-\alpha C)}\right]M^2(1-\alpha^2C^2)\right.$$
$$\left.+C^2(1-M\alpha u)^2\left[1-\frac{v}{w}\frac{J_n'(kav)\,H_n^{(2)}(kaw)}{J_n(kav)\,H_n'^{(2)}(kaw)}\right]\right\}. \quad (3.10)$$

Since the zero has to lie in the region $\operatorname{Im} v > 0$ we have

$$v(u_5) = w(u_5) = i[(1+C)^2 - M^2C^2(1-\alpha)^2]^{\frac{1}{2}}/(1+\alpha C)\,M.$$

Then from the high frequency approximation to (3.10) we can derive

$$u_5 = \frac{1+C}{M(1+\alpha C)} + \frac{(-1)^n iC(1-\alpha)}{(1+\alpha C)^2 M}\exp\left\{\frac{-2ka}{M(1+\alpha C)}[(1+C)^2 - M^2C^2(1-\alpha^2)]^{\frac{1}{2}}\right\}.$$

For $n$ odd the zero lies below the branch cut on the physical Riemann sheet. However when $n$ is even it lies on the other Riemann sheet and above the branch cut. So only for $n$ odd is this zero relevant.

Now consider the position of $u_4$. It lies on the real line but whether or not it is positioned on a branch cut is dependent upon the values of the parameters. We find that

(i) if $[1+M(1-\alpha)]^{-1} < C < [1-M(1-\alpha)]^{-1}$ then $u_4$ lies between the branch points,

(ii) if $C < [1+M(1-\alpha)]^{-1}$ or $C > \alpha^{-1}$ then $u_4$ lies on the branch cut to the right of $1/(1+M)$ and $C/(1+M\alpha C)$, and

(iii) if $[1-M(1-\alpha)]^{-1} < C < \alpha^{-1}$ then $u_4$ lies on the branch cut to the left of $-1/(1-M)$ and $-C/(1-M\alpha C)$.

For case (i) the condition $\operatorname{Im} v > 0$ is violated and so a zero is not obtained. Cases (ii) and (iii) may be treated in a similar way to $u_5$. In these cases a better approximation to $u_4$ is

$$u_4 = \frac{1-C}{M(1-\alpha C)} - \frac{(-1)^n iC(1-\alpha)}{M(1-\alpha C)^2}\exp\left\{\frac{-2ka}{M}\left|\frac{(1-C^2)-C^2M^2(1-\alpha^2)}{(1-\alpha C)^2}\right|^{\frac{1}{2}}\right\}.$$

Therefore the zero lies on the physical Riemann sheet in case (ii) only for $n$ even, when it is below the branch cut, and in case (iii) only for $n$ odd, when it lies above the branch cut.

All the zeros just discussed lie in the region $|\operatorname{Im}(kav)| \gg 1$. The remaining region consists of a narrow strip about the line $\operatorname{Re} u = -M/(1-M^2)$ and a strip about the real axis including the branch points $-1/(1-M)$ and $1/(1+M)$. There are an infinite number of zeros and poles of $\chi$ in this region. The poles correspond to zeros of $J_n'(kav)$.

A finite number of these lie on the real line between the branch points $-1/(1-M)$ and $1/(1+M)$. The remainder are located on the line $\mathrm{Re}\, u = -M/(1-M^2)$.

There are no zeros of $\chi$ anywhere on the real line except when case I and/or case II occurs. In case I, since $\chi$ is imaginary on the bottom of the branch between $-1/(1-M)$ and $-C/(1-M\alpha C)$, there may be zeros of $\chi$ here and these will in general be interlaced between those of $J_n'(kav)$. A similar result holds in case II for zeros on the real line above the branch cut between $C/(1+M\alpha C)$ and $1/(1+M)$.

In the narrow strip about $\mathrm{Re}\, u = -M/(1-M^2)$ and where $|Mu|$, $|kav|$ and $|kaw|$ are much larger than unity the zeros of $\chi$ are close to solutions of

$$\cot(kav - \tfrac{1}{2}n\pi - \tfrac{1}{4}\pi) = -i\gamma v\alpha^2/w. \tag{3.11}$$

For sufficiently large $|Mu|$, in the strip, $\mathrm{Re}\,(v/w) > 0$. Also $\mathrm{Im}\{\cot(kav - \frac{1}{2}n\pi - \frac{1}{4}\pi)\}$ has the opposite sign to $\mathrm{Im}\, v$. Therefore one deduces that, for $|Mu| \gg 1$, any zeros of $\chi$ close to $\mathrm{Re}\, u = -M/(1-M^2)$ lie to the left of this line above the real axis, whilst those below lie to the right. These zeros will be near to the intersection of the curve $\mathrm{Re}\,\chi = 0$ with $\mathrm{Re}\, u = -M/(1-M^2)$, which occurs between the consecutive zeros of $J_n'(kav)$.

We complete the qualitative discussion of the position of zeros for real $k$ by briefly observing their positions for $|ka| \ll 1$. In the region $|uka| \ll 1$ the zeros of (3.2) are close to

$$u = \begin{cases} \dfrac{\gamma\alpha+1}{M(1+\gamma\alpha^2)} \pm \dfrac{i}{M}\dfrac{(1-\alpha)}{(1+\gamma\alpha^2)}\gamma^{\frac{1}{2}}, & n \neq 0, \\ \dfrac{1}{M} \pm i\dfrac{\gamma^{\frac{1}{2}}(1-\alpha)\,ka}{2^{\frac{1}{2}}M^2}\,|\ln(ka)|^{\frac{1}{2}}, & n = 0. \end{cases}$$

For $|Muka| \gg 1$ the zeros essentially satisfy (3.11) and, as discussed in the previous paragraph, are confined to a strip about $\mathrm{Re}\, u = -M/(1-M^2)$.

On figures 1 (*a*)–(*d*) we have numerically located the zeros of $L(u,k)$, where

$$L(u,k) = \chi(-iku)/vw, \tag{3.12}$$

for real $k$, $n = 0$ and different values of $\alpha$ and $C$. The zeros of $\chi$ are of course the same as those of $L(u,k)$. Figures 1 (*a*)–(*c*) illustrate the typical positioning of the zeros in case I and figure 1 (*d*) the positioning for

$$-C/(1-M\alpha C) < -1/(1-M) < 1/(1+M) < C/(1+M\alpha C).$$

On all these figures we have superimposed the curves $\mathrm{Re}\, L = 0$ and $\mathrm{Im}\, L = 0$. A picture emerges of the way the zeros and poles are linked, the curves being discontinuous at the poles of $L$. In general there is only one zero in the region $\mathrm{Re}\, u, \mathrm{Im}\, u > 0$. This is clearly seen in these figures and is close to $u_0$ for $|ka| \gg 1$. As predicted from (3.8) this zero moves towards the real axis as $\alpha$ approaches unity as can be verified by comparing figures 1 (*a*) and (*b*). However there is not always only one zero in $\mathrm{Re}\, u$, $\mathrm{Im}\, u > 0$. One or more of the system of zeros near the line $\mathrm{Re}\, u = -M/(1-M^2)$ may encroach into this region for sufficiently small $M$ and $|Mkau|$. Crow & Champagne (1971) and Lee & Jones (1973) have discovered these additional zeros and one case is shown in figure 2.

Of particular relevance to the question of causality, discussed in § 5, is the location of the zeros of $\chi$ for complex $k$ and $0 < \delta < \pi$. When $k$ is negative imaginary, i.e. $\delta = \frac{1}{2}\pi$, all the poles of $L(u,k)$ lie on the real axis in the $u$ plane. Therefore the number of zeros

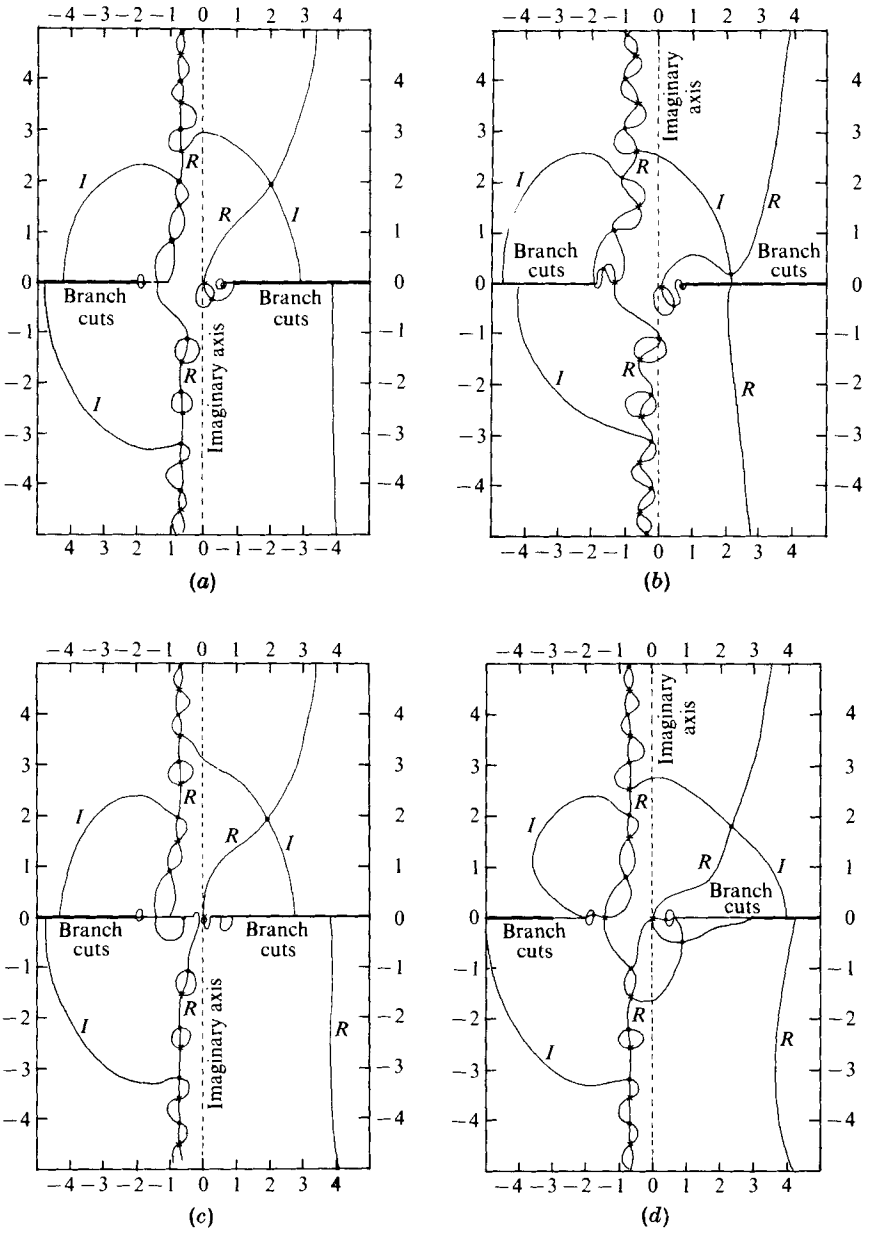


FIGURE 1. Behaviour of $L(u, k)$ in the complex $u$ plane. ●, zeros of $L$; *, poles of $L$. $n = 0$, $M = 0{\cdot}5$, $ka = 4{\cdot}0$, $\gamma = 1{\cdot}0$. (*a*) $\alpha = 0$, $C = 1{\cdot}0$. (*b*) $\alpha = 0{\cdot}9$, $C = 1{\cdot}0$. (*c*) $\alpha = 0$, $C = 0{\cdot}2$. (*d*) $\alpha = 0$, $C = 3{\cdot}0$. $R$ and $I$ indicate where Re $L = 0$ and Im $L = 0$ respectively.

of $L(u, k)$ in the upper half $u$ plane is related to the change in arg $L$ on the closed contour consisting of a semicircle at infinity and the contour just above the real axis passing over all branch points, poles and zeros occurring on the real axis. On the semicircle

$$u = \lim_{R \to \infty} \mathrm{Re}^{i\theta}, \quad 0 < \theta < \pi, \tag{3.13}$$

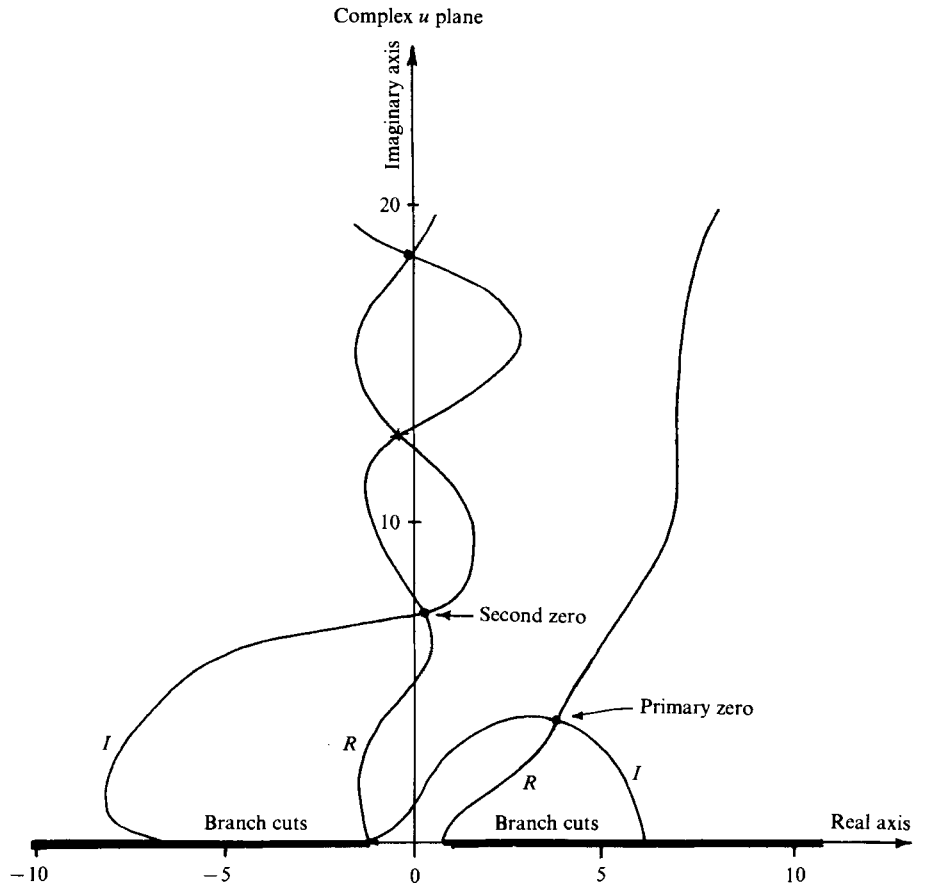


FIGURE 2. Possibility of more than one zero of $L(u, k)$ in the region Re $u$, Im $u > 0$. $n = 0$, $M = 0{\cdot}2$, $\alpha = 0$, $ka = 0{\cdot}3$, $\gamma = C = 1{\cdot}0$.

a straightforward analysis reveals that on the arc given by $0 < \epsilon_1 < \theta < \pi - \epsilon_1$, where $\epsilon_1 \to 0$ and $R\epsilon_1|k|a(1-M^2)^{\frac{1}{2}} \gg 1$, $\arg L$ increases by $\pi - 2\epsilon_1$ as $\theta$ increases from $\epsilon_1$ to $\pi - \epsilon_1$. On the remaining portion of the contour the analysis is a little more complicated. Let $C$ denote the point $u = -1/(1+M) + i\epsilon_2$, $D$ denote the point $u = 1/(1+M) + i\epsilon_2$ and $A$, $B$, $E$ and $F$ denote the points on the semicircle (3.13) corresponding to $\theta = \pi - \epsilon_1$, $\pi$, 0 and $\epsilon_1$, respectively. If we assume $\arg L = \frac{1}{2}\pi$ at $u = 0$ then by careful inspection of $\arg L$ we can show that

$$(1)\ -\tfrac{1}{2}\pi < \arg L < \tfrac{1}{2}\pi \quad \text{on the contour } ABC,$$

$$(2)\ \tfrac{1}{2}\pi < \arg L < \tfrac{3}{2}\pi \quad \text{on the contour } DEF.$$

In particular $\arg L = 0$ at $A$ and $\arg L = \pi$ at $F$. Hence $\arg L$ increases by $\pi$ around the contour $ABCDEF$. Therefore, since the total change in $\arg L$ is $2\pi$ on the closed contour there can be one and only one zero $\hat{u}_0(k)$, say, of $L$ in the upper half-plane when $\delta = \frac{1}{2}\pi$. Further, its position will tend to $u_0$ as $|ka| \to \infty$. Using the property

$$L^*(u, k) = -L(u^*, -k^*), \tag{3.14}$$

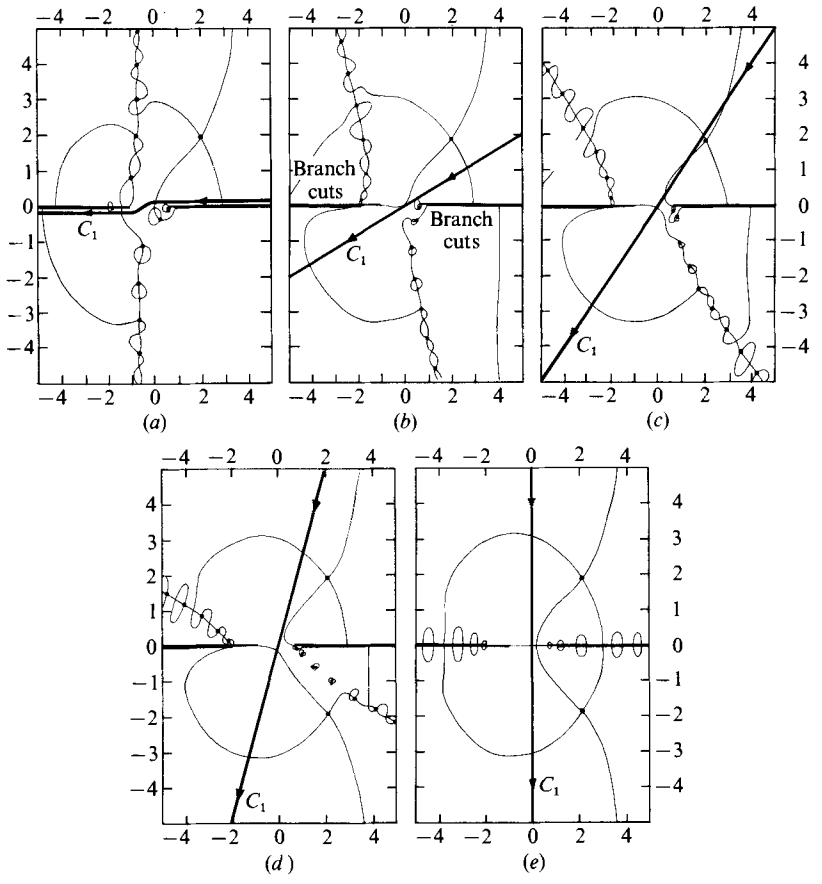


FIGURE 3. Complex $u$ plane. Position of the zeros of $L(u, k)$ (solid circles) and the contour $C_1$ as arg $k = -\delta$ varies. $n = 0$, $M = 0{\cdot}5$, $\alpha = 0$, $|ka| = 4{\cdot}0$, $\gamma = C = 1{\cdot}0$. (*a*) $\delta = 0$, (*b*) $\delta = \frac{1}{8}\pi$, (*c*) $\delta = \frac{1}{4}\pi$, (*d*) $\delta = \frac{3}{8}\pi$, (*e*) $\delta = \frac{1}{2}\pi$.

where an asterisk indicates the complex conjugate, one deduces that there is only one zero in the lower half-plane. This is at $\hat{u}_0^*(k)$. Of course the zeros $\hat{u}_0$ and $\hat{u}_0^*$ are also zeros of $\chi(u, k)$.

Rather than pursue a further qualitative, and necessarily lengthy, discussion we shall revert to a numerical description of the location of the zeros for other values of $\delta$. The typical behaviour of the zeros for $0 < \delta < \frac{1}{2}\pi$ is shown in figure 3. One can extend this illustration to $\frac{1}{2}\pi < \delta < \pi$ by a simple application of (3.14); i.e. the zeros for $\delta = \theta$ are the complex conjugates of those for $\delta = \pi - \theta$.

Let $C_1$ be the contour Im $(ku) = 0$, $-\infty < |u| < \infty$; then an important question, related to causality, is when does a zero of $\chi$ lie on $C_1$? The typical situation is illustrated by referring to figure 3. By tracing the zeros in the $u$ plane for $0 < \delta < \frac{1}{2}\pi$ we see that only $\hat{u}_0(k)$ can ever lie on $C_1$. Similarly its conjugate $\hat{u}_0^*(k)$ is the only zero that can lie on this line for $\frac{1}{2}\pi < \delta < \pi$. Particular note should be made of the trace of the system of zeros that were near $-M/(1-M^2)$ for $\delta = 0$. In all cases considered these never cross $C_1$. The same result is true of the additional zero shown in figure 2. A plot of the dependence of $\hat{u}_0(k)$ on $\delta$ for $0 < \delta < \frac{1}{2}\pi$ is given in figure 4 for a range of values of $\alpha$ for fixed

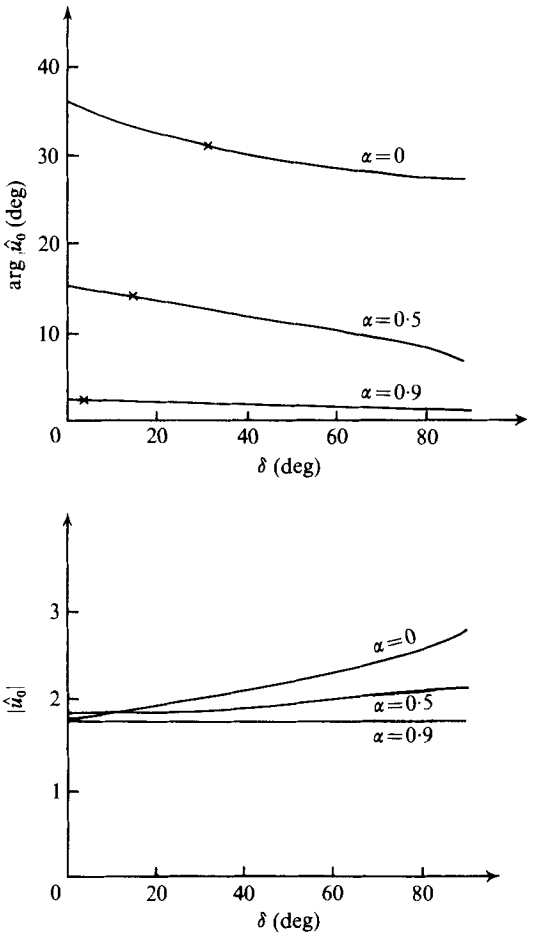


FIGURE 4. Dependence of position of instability pole $\hat{u}_0(k)$ on arg $k = -\delta$ for $\alpha = 0$, 0·5 and 0·9, $n = 0$, $M = 0{\cdot}6$, $|ka| = 0{\cdot}6$, $C = \gamma = 1{\cdot}0$.

$|ka| = 0{\cdot}6$. It appears, from a detailed numerical search throughout a wide range of parameters, that the zero $\hat{u}_0(k)$ is crossed only once by $C_1$ and that this is for $\delta$ in $0 < \delta < \frac{1}{2}\pi$. We shall therefore assume that this is always the case.

Finally define $C_0$ as the contour in the lower half $k$ plane for which a zero of $\chi$ is situated on $C_1$. This contour $C_0$ is shown in figure 5 for different values of $\alpha$ and $C$. Also illustrated is the region $\Delta_0$, which includes the whole of the negative imaginary axis and is bounded by $C_0$. These will be referred to again in § 5.

## 4. The split functions

The split functions $\chi_+(s)$ and $\chi_-(s)$ were formally introduced in § 2 to enable the Wiener–Hopf equation to be solved. In this section we shall derive explicit expressions for these functions suitable for numerical calculations. The derivation is not subject to any approximations.

In general when $k$ has a small negative imaginary part there are no zeros of $\chi(s)$ in

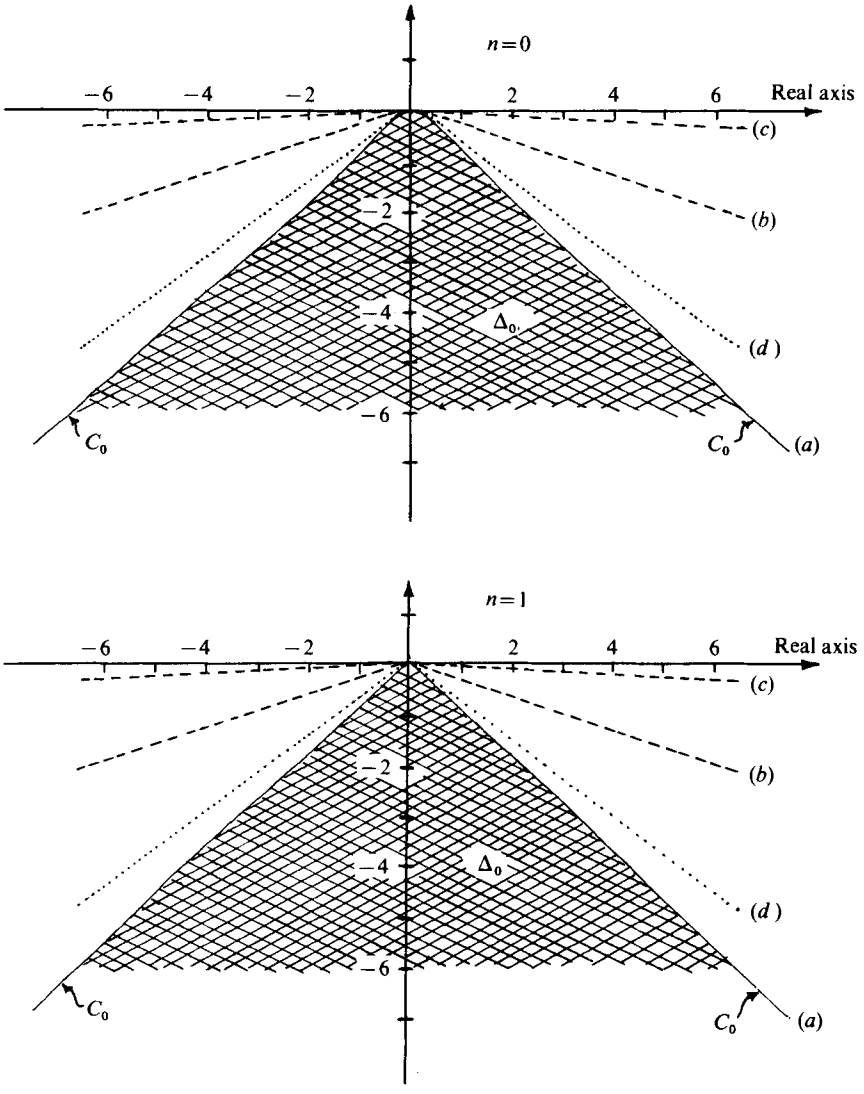


FIGURE 5. The region $\Delta_0$ and the contour $C_0$ in the lower half of the complex $k$ plane for $n = 0$ and 1, $M = 0{\cdot}5$, $\gamma = 1$ and (*a*) $\alpha = 0$, $C = 1{\cdot}0$, (*b*) $\alpha = 0{\cdot}5$, $C = 1{\cdot}0$, (*c*) $\alpha = 0{\cdot}9$, $C = 1{\cdot}0$, (*d*) $\alpha = 0$, $C = 3{\cdot}0$.

the strip $s_1 < \operatorname{Re} s < s_2$, and $\arg\chi(-i\infty) = \arg\chi(i\infty)$. Therefore on integrating $\ln\chi(s)/(s-x)$ around a rectangular contour with vertices $b_1 \pm i\infty$ and $b_2 \pm i\infty$ such that $s_1 < b_1 < \operatorname{Re} x < b_2 < s_2$, the result is

$$\ln\chi(x) = \ln\chi_+(x) - \ln\chi_-(x), \tag{4.1}$$

where

$$\ln\chi_+(x) = -\frac{1}{2\pi i}\,\mathrm{P}\int_{b_1-i\infty}^{b_1+i\infty}\frac{\ln\chi(s)}{s-x}\,ds$$

and

$$\ln\chi_-(x) = -\frac{1}{2\pi i}\,\mathrm{P}\int_{b_2-i\infty}^{b_2+i\infty}\frac{\ln\chi(s)}{s-x}\,ds.$$

Here 'P' means that we evaluate the integral as both ends of the contour tend to infinity simultaneously. However, as mentioned in the preceding section, when $\delta$ varies and $\alpha < 1$ there will be a value of $\delta$ such that the zero $s_0 = -iku_0$ lies on the imaginary axis of the $s$ plane and therefore in the strip $s_1 < \mathrm{Re}\, s < s_2$. In particular, for the high frequency limit with $C = \gamma = 1$ this value of $\delta$ is given by

$$\tan\delta = \eta(1-\alpha)/\xi(1+\alpha).$$

The necessary modifications to (4.1) that are needed to account for a zero in the strip are described by Noble (1958, p. 41).

Let us restrict considerations to $\alpha < 1$ and small $\delta$. Then (4.1) is still valid and so

$$\chi(s) = \chi_+(s)/\chi_-(s), \tag{4.2}$$

where $\chi_+(s)$ is regular and non-zero for $\mathrm{Re}\, s > s_1$ and $\chi_-$ is regular and non-zero for $\mathrm{Re}\, s < s_2$. One can easily deduce the properties

$$\chi_+(s) = O(s^{\frac{1}{2}}), \quad \chi_-(s) = O(s^{-\frac{1}{2}}) \tag{4.3}$$

as $|s| \to \infty$ in appropriate half-planes.

Now put $k_i = 0$ and make the transformation $s = -iku$. Then for real $y$

$$\ln\chi_+(-iky) = \frac{1}{2\pi i}\mathrm{P}\int_{-\infty}^{\infty} \frac{\ln\chi(-iku)}{u-y}\,du + \tfrac{1}{2}\ln\chi(-iky) \tag{4.4}$$

and

$$\ln\chi_-(-iky) = \frac{1}{2\pi i}P\int_{-\infty}^{\infty} \frac{\ln\chi(-iku)}{u-y}\,du - \tfrac{1}{2}\ln\chi(-iky), \tag{4.5}$$

where P now indicates the Cauchy principal value of the integral. The contour of integration $-C_1$ in each case passes along the bottom edge of the branch cuts from $-\infty$ and along the top edge of the branch cuts from $+\infty$. The contour is shown in figure 3 (*a*).

Our main interest is in the magnitude of diffracted sound for each mode of propagation. Therefore we shall restrict consideration to the calculation of the quantities $|\chi_+|$ and $|\chi_-|$. In particular $|\chi_+|$ is given by

$$\ln|\chi_+(-iky)| = \frac{1}{2\pi}P\int_{-d_1}^{d_2} \frac{\arg\chi(-iku)}{u-y}\,du + \tfrac{1}{2}\ln|\chi(-iky)|, \tag{4.6}$$

where $$d_2 = \max\left[\frac{1}{1+M}, \frac{C}{1+M\alpha C}\right], \quad d_1 = \max\left[\frac{1}{1-M}, \frac{C}{1-M\alpha C}\right].$$

It is convenient at this stage to write

$$\chi(-iku) = E(u)/K(u),$$

where $$E(u) = \gamma(1-M\alpha u)^2 v H_n^{(2)}(kaw)\,J_n'(kav) - (1-Mu)^2 w J_n(kav)\,H_n'^{(2)}(kaw)$$

and $$K(u) = J_n'(kav)\,H_n'^{(2)}(kaw).$$

The splitting of $|\chi(-iku)|$ could be achieved directly without reference to $E$ and $K$. However it proves less confusing to deal with $E$ and $K$ instead of $\chi$. Equations similar to (4.4) and (4.5) also hold for splittings of $E$ and $K$, so that

$$\chi_+(-iky) = E_+(y)/K_+(y), \quad \chi_-(-iky) = E_-(y)/K_-(y).$$

Consider first the function $|K_+|$. If there are $l$ zeros of $J_n'(kav)$ in the range 0 to $ka/(1-M^2)^{\frac{1}{2}}$ then it is not too difficult to show that

$$|K_+(y)| = \left| J_n'(kav)\, H_n'(kaw) \prod_{j=1}^{l} \left( \frac{a_j - y}{a_j + y + 2M/(1-M^2)} \right) \right|^{\frac{1}{2}} \times \exp\left\{ I_1 - \left[ \frac{\arg H_n'(kaw)}{\pi} - \frac{n}{4} \right] \ln \left| \frac{y + C/(1-M\alpha C)}{y - C/(1+M\alpha C)} \right| + A_1 \ln \left| \frac{y - 1/(1+M)}{y + 1/(1-M)} \right| \right\}, \tag{4.7}$$

where

$$A_1 = \begin{cases} \frac{1}{4}, & n = 0, \\ \frac{1}{4}(n-1) & n \neq 0, \end{cases}$$

$$I_1 = \left[ \frac{y + MC^2\alpha/(1-M^2\alpha^2C^2)}{\pi} \right] \int_0^{C/(1-M^2\alpha^2C^2)} \frac{\arg H_n'^{(2)}(ka\hat{w}(z)) - \arg H_n'^{(2)}(kaw(y))}{z^2 - [y + C^2M\alpha/(1-M^2\alpha^2C^2)]^2}\, dz, \tag{4.8}$$

$$\hat{w}(z) = (1-M^2\alpha^2C^2)^{\frac{1}{2}} \{ C^2/(1-M^2\alpha^2C^2)^2 - z^2 \}^{\frac{1}{2}}$$

and

$$a_l = \left\{ \left[ 1 - (1-M^2) \left( \frac{j_{n,l}'}{ka} \right)^2 \right]^{\frac{1}{2}} - M \right\} \Big/ (1-M^2).$$

Here we have taken $\arg H_n'^{(2)}(ka\hat{w}(z))$ as $-\frac{1}{2}\pi$ at $z = C/(1-M^2\alpha^2C^2)$.

The function $E_+(y)$ needs more care since $\arg E(y)$ is discontinuous at the branch points. As the contour $-C_1$ passes under $-1/(1-M)$ the function $\arg E(u)$ increases by $\frac{1}{2}n\pi$ whilst at $-C/(1-M\alpha C)$ it decreases by $\frac{1}{2}n\pi$. Similarly $\arg E(u)$ increases by $\frac{1}{2}n\pi$ as $-C_1$ passes over $C/(1+M\alpha C)$ and decreases by $\frac{1}{2}n\pi$ over $1/(1+M)$. To assist with the numerical work let us define a new function $\arg \hat{E}(u)$ that has the same value close to and on either side of the branch points by

$$\arg \hat{E}(u) = \arg E(u) + \frac{n\pi}{2} \left[ H\left( u - \frac{1}{1+M} \right) - H\left( u + \frac{1}{1-M} \right) - H\left( u - \frac{C}{1+M\alpha C} \right) + H\left( u + \frac{C}{1-M\alpha C} \right) \right],$$

where $H(x)$ is the unit Heaviside function. Then

$$|E_+(y)| = |E(y)|^{\frac{1}{2}} \exp\left\{ B_1 + B_2 + B_3 + \left[ \frac{\arg \hat{E}(y)}{2\pi} - \frac{1}{4} \right] \ln \left| \frac{d_2 - y}{d_1 - y} \right| + \frac{n}{4} \ln \left| \frac{[y - 1/(1+M)]\,[y + C/(1-M\alpha C)]}{[y + 1/(1-M)]\,[y - C/(1-M\alpha C)]} \right| \right\}, \tag{4.9}$$

where

$$B_1 = \frac{1}{2\pi} \int_{-C/(1-M\alpha C)}^{C/(1+M\alpha C)} \frac{\arg \hat{E}(u) - \arg \hat{E}(y)}{u - y}\, du, \tag{4.10}$$

$$B_2 = \begin{cases} \dfrac{1}{2\pi} \displaystyle\sum_{i=1}^{m_1+1} \phi_i \ln \left| \frac{\gamma_i - y}{\gamma_{i-1} - y} \right| & \text{for case I,} \\ 0 & \text{otherwise,} \end{cases}$$

$$B_3 = \begin{cases} \dfrac{1}{2\pi} \displaystyle\sum_{i=1}^{m_2+1} \hat{\phi}_i \ln \left| \frac{\hat{\gamma}_i - y}{\hat{\gamma}_{i-1} - y} \right| & \text{for case II,} \\ 0 & \text{otherwise.} \end{cases}$$

Here $\gamma_i$ and $\hat{\gamma}_i$ are the zeros of $\chi(-iku)$ that appear on the branch cuts if case I or case II occurs, respectively.

These zeros have been arranged such that

$$-\frac{1}{1-M} < \gamma_1 < \gamma_2 < \ldots < \gamma_{m_1} < -\frac{C}{1-M\alpha C}, \quad \frac{C}{1+M\alpha C} < \hat{\gamma}_1 < \ldots < \hat{\gamma}_{m_2} < \frac{1}{1+M}.$$

The function $\arg \hat{E}(u)$ is a constant between consecutive zeros. In general $\arg \hat{E}$ increases by $\pi$ on the contour as $u$ passes under $\gamma_i$ and decreases by $\pi$ as $u$ passes over $\hat{\gamma}_i$. Then

$$\phi_j = \tfrac{1}{2}\pi + (j-1)\pi - \arg \hat{E}(y) \quad \text{for} \quad \gamma_{j-1} < u < \gamma_j$$

and

$$\hat{\phi}_j = \tfrac{1}{2}\pi + (m_2 - j + 1)\pi - \arg \hat{E}(y) \quad \text{for} \quad \hat{\gamma}_{j-1} < u < \hat{\gamma}_j,$$

where $\gamma_{m_1+1} = -\dfrac{C}{1-M\alpha C}$, $\gamma_0 = -\dfrac{1}{1-M}$, $\hat{\gamma}_{m_2+1} = \dfrac{1}{1+M}$, $\hat{\gamma}_0 = \dfrac{C}{1+M\alpha C}$.

However, as a necessary precaution, one should include in the calculation of $\phi_j$ the possibility that the contour actually passes over and not under $\gamma_j$. This occurs if

$$\left[k\frac{\partial \chi}{\partial k}\Big/\frac{\partial \chi}{\partial u} - u\right]_{u=\gamma_j} < 0;$$

then $\arg \hat{E}(u)$ will decrease by $\pi$ on the contour as $u$ passes *over* $\gamma_j$. The required modifications are easily built into the calculation of $\arg \hat{E}(u)$ and $\phi_j$.

## 5. Causality

In this section the causality of the sound field is investigated. Jones & Morgan (1972) approached this problem by analysing the initial-value problem in the space of ultra-distributions (Jones 1973) and requesting that the sound field should not exist before the source is triggered. Their analysis showed that, to make the solution to the harmonic problem causal, one needed to add a homogeneous solution to it and this gave rise to instability waves. This approach to causality can be analysed explicitly for problems involving plane vortex sheets but, unfortunately, is difficult to implement when cylindrical vortex layers are involved.

There is, however, a theorem on causality, derived by Jones & Morgan (1974), that can be applied directly to the harmonic problem.

THEOREM. Let $\phi(k)$ be a solution to a harmonic problem with time dependence $\exp(ikc_j t)$. Then $\phi(k)$ is causal if and only if it is a regular function of $k$ in $\operatorname{Im} k < 0$ and there exist real constants $b$ and $d > 0$ such that

$$\exp[(b+id)k]\,\phi(k) = O(|k|^p) \tag{5.1}$$

as $|k| \to \infty$ in $\operatorname{Im} k < \epsilon < 0$ for some finite $p$.

This theorem has been successfully applied by Morgan (1974, 1975) and we shall use it in a similar manner. First it is shown that (2.22) is the only causal solution for $\delta = \frac{1}{2}\pi$ and $|k|$ sufficiently large. Then $\psi$ is made into a regular function in the complete lower half $k$ plane. Finally we verify that the causal solution we have constructed satisfies the necessary boundary conditions when $\delta = 0$.

For $\delta = \frac{1}{2}\pi$ the two zeros $\hat{u}_0(k)$ and $\hat{u}_0^*(k)$ of $\chi$ lie in the region

$$\operatorname{Re} u > \operatorname{Im}(u)\cot\delta + |\hat{\epsilon}|,$$

for some small $\hat{\epsilon} \neq 0$; see figure 3(*e*). Denote the corresponding zeros in the $s$ plane by $s_0(k)$ and $s_0^*(k)$ and define $\hat{\mu}(s)$ by

$$\chi(s) = (s-s_0)(s-s_3)\hat{\mu}(s), \tag{5.2}$$

where $s_3 = s_0^*$ when $\delta = \frac{1}{2}\pi$.

In the high frequency case, $|ka| \gg 1$, with $\delta = \frac{1}{2}\pi$ it is a simple matter to verify that there is no change in $\arg \hat{\mu}(s)$ on the imaginary axis between $s = \pm i\infty$. For other values of $|k|$ it has not been possible to prove analytically that $\arg \hat{\mu}(s)$ has the same value at these ends of the contour on the imaginary axis. However a numerical search suggests that there is no change in $\arg \hat{\mu}(s)$ and so this will be assumed throughout the remaining analysis. Therefore the splitting (4.1) can be applied to $\hat{\mu}(s)$ to give

$$\hat{\mu}(s) = \hat{\mu}_+(s)/\hat{\mu}_-(s).$$

Then $$\chi_+(s) = (s-s_0)(s-s_3)\hat{\mu}_+(s), \quad \chi_-(s) = \hat{\mu}_-(s).$$

Also $\hat{\mu}_+(s) = O(s^{\frac{1}{2}})$ and $\hat{\mu}_-(s) = O(s^{-\frac{1}{2}})$ as $|s| \to \infty$ in the appropriate half-planes.

Substituting $\chi(s)$ from (5.2) into (2.17) and applying the Wiener–Hopf technique, as in § 2, with the bounds appropriate to $\delta = \frac{1}{2}\pi$ we obtain

$$F_+(s) = \frac{-i(k-\mu M)\hat{\mu}_-(-i\mu)\lambda_1^-(-i\mu)\lambda_2^-(-i\mu)\lambda_1^+(s)\lambda_2^+(s)}{2\pi c_j k^3(s+i\mu)(s-s_0)(s-s_3)\hat{\mu}_+(s)}. \tag{5.3}$$

This is identical to the value given by (2.21). The field in $r > a$ equivalent to (2.22) is

$$\psi(r,z) = \frac{1}{2\pi i}\int_{e-i\infty}^{e+i\infty} \frac{c_j(ik+M\alpha s)F_+(s)H_n^{(2)}(\lambda_2 r)}{\lambda_2 H_n'^{(2)}(\lambda_2 a)} \exp(sz)\,ds, \tag{5.4}$$

where $$s_1 < e < s_2 \quad \text{and} \quad \delta = \tfrac{1}{2}\pi.$$

Taking the limit of high frequency, $|k| \gg 1$, with $\delta = \frac{1}{2}\pi$ and $s = -iku$ equation (5.4) becomes

$$\psi(r,z) \sim \frac{1}{2\pi}\int_{-i\infty}^{i\infty} \frac{K_2[1-u(1+M)]^{\frac{1}{2}}[C-u(1+M\alpha C)]^{\frac{1}{2}}(1-M\alpha u)a^{\frac{1}{2}}}{(u-\mu/k)(u-u_0)(u-u_0^*)\hat{\mu}_+(-iku)wr^{\frac{1}{2}}} \times \exp[-ikw(r-a)-ikuz]\,du, \tag{5.5}$$

where $$K_2 = -\frac{1}{2\pi k^2}\left(1-\frac{\mu}{k}M\right)\hat{\mu}_-(-i\mu)\left[1+\frac{\mu}{k}(1-M)\right]^{\frac{1}{2}}\left[C+\frac{\mu}{k}(1-M\alpha C)\right]^{\frac{1}{2}}.$$

Now with $\delta = \frac{1}{2}\pi$ and sufficiently large $|k|$,

$$\chi(-iku) \sim i\Lambda(u),$$

where $\Lambda(u) = \gamma(1-M\alpha u)^2 v + (1-Mu)^2 w$. When $\gamma = C = 1$ and $\alpha = 0$ this is the function $\Lambda$ that arises for the plane vortex sheet problem of Jones & Morgan (1972). The splitting of this is given by Morgan (1974) and is essentially the splitting of $\chi$ when $|k| \to \infty$. One observes that the integrand in (5.5) is similar to that encountered in the semi-infinite vortex sheet problem discussed by Morgan (1975). It is known in that problem that the solution is causal for $\delta = \frac{1}{2}\pi$. Therefore when $|k|$ is sufficiently large the solution (5.5) is also causal for $\delta = \frac{1}{2}\pi$.

That this is a unique solution can be easily verified. Any other solution must differ from (5.5) by a linear combination of the residues at the poles of the integrand. Since

all the poles lie in the region $\mathrm{Re}\, u > 0$ it follows that, when $z$ is sufficiently large and negative, $d$ in the theorem must be negative. So such a solution cannot be causal.

It can be verified that the integral (5.4) converges uniformly with respect to $k$ when $k$ lies within the region $\Delta_0$ defined in § 3 and shown in figure 5. Therefore $\psi$ is a regular function of $k$ in $\Delta_0$ and is the analytic continuation of the solution for $|k|$ sufficiently large and $\delta = \frac{1}{2}\pi$. Hence, from the theorem, $\psi$ is causal throughout the region $\Delta_0$.

Now across $C_0$ and for $0 < \delta < \frac{1}{2}\pi$ the pole $s_0(k)$ of the integrand is encountered. Similarly $s_3 = s_0^*$ is encountered on $C_0$ for $\frac{1}{2}\pi < \delta < \pi$. In either case $\psi$ is discontinuous across $C_0$. Thus to meet the regularity requirement of the theorem we define a new function $\psi^c$ by removing the singularity in $\psi$: viz.

$$\psi^c(r,z) = \frac{1}{2\pi i}\int_{e-i\infty}^{e+i\infty} \frac{c_j(ik+M\alpha s)\,F_+(s)\,H_n^{(2)}(\lambda_2 r)\exp(sz)}{\lambda_2 H_n'^{(2)}(\lambda_2 a)}\,ds + \hat{H}(\Delta_0)\lim_{s\to\hat{s}_0(k)}\left[\frac{c_j(ik+M\alpha s)\,F_+(s)\,(s-\hat{s}_0)\,H_n^{(2)}(\lambda_2 r)}{\lambda_2 H_n'^{(2)}(\lambda_2 a)}\right]\exp(\hat{s}_0 z), \quad r > a, \tag{5.6}$$

where
$$\hat{s}_0 = \begin{cases} s_0 & \text{if } 0 < \delta < \frac{1}{2}\pi, \\ s_0^* & \text{if } \frac{1}{2}\pi < \delta < \pi, \end{cases} \qquad \hat{H}(\Delta_0) = \begin{cases} \frac{1}{2} & \text{if } k \in C_0, \\ 0 & \text{if } k \in \Delta_0, \\ 1 & \text{otherwise.} \end{cases}$$

The solution $\psi^c$ is now causal for all $k$ in the lower half $k$ plane.

By a similar process one can derive the solution which is causal for $r < a$. In particular, when $\mathrm{Re}\, k > 0$ and $\delta \to 0$

$$\psi^c(r,z) = \begin{cases} \dfrac{1}{2\pi i}\displaystyle\int_{e-i\infty}^{e+i\infty} \frac{c_j(ik+Ms)\,F_+(s)\,J_n(\lambda_1 r)}{\lambda_1 J_n'(\lambda_1 a)}\exp(sz)\,ds \\ \quad + \left[\dfrac{c_j(ik+Ms)\,F_+(s)\,(s-s_0)\,J_n(\lambda_1 r)}{\lambda_1 J_n'(\lambda_1 a)}\right]_{s=s_0(k)}\exp(s_0 z), \quad r < a, \qquad (5.7a) \\ \dfrac{1}{2\pi i}\displaystyle\int_{e-i\infty}^{e+i\infty} \frac{c_j(ik+M\alpha s)\,F_+(s)\,H_n^{(2)}(\lambda_2 r)}{\lambda_2 H_n'^{(2)}(\lambda_2 a)}\exp(sz)\,ds \\ \quad + \left[\dfrac{c_j(ik+M\alpha s)\,F_+(s)\,(s-s_0)\,H_n^{(2)}(\lambda_2 r)}{\lambda_2 H_n'^{(2)}(\lambda_2 a)}\right]_{s=s_0(k)}\exp(s_0 z), \quad r > a. \qquad (5.7b) \end{cases}$$

There is no difficulty in establishing that $\psi^c(r,z)$, as given by (5.7), satisfies the boundary conditions (2.4) and (2.5). To verify that (2.3) is satisfied first observe that the non-exponential parts in the integrands that arise in $\partial\psi^c(a,z)/\partial r$, derived from (5.7), are $O(|s|^{-\frac{1}{2}})$ as $|s| \to \infty$ in $\mathrm{Re}\, s > s_1$. Then the required result is confirmed by closing the contours in the right half-plane for $z < 0$; viz.

$$\partial\psi^c(a,z)/\partial r = 0 \quad \text{for} \quad z < 0.$$

Consider now the Kutta condition at the edge of the cylinder. Let $h^c(z)$ denote the causal displacement of the vortex layer. Then for $\delta \to 0$

$$h^c(z) = \frac{1}{2\pi i}\int_{e-i\infty}^{e+i\infty} F_+(s)\exp(sz)\,ds + (s-s_0)\,F_+(s_0)\exp(s_0 z). \tag{5.8}$$

Here $F_+(s)$ is $O(|s|^{-\frac{5}{2}})$ as $|s| \to \infty$ and so the integral for $h^c(z)$ is a uniformly convergent function of $z$. $h^c(z)$ is therefore a continuous function for all $z$. Since the contour can be closed in the right half-plane to give $h^c(z) = 0$ for $z < 0$, this implies that $h(z) \to 0$ as $z \to 0^+$. The same is true of $dh^c(z)/dz$ but $d^2h^c(z)/dz^2$ is discontinuous at $z = 0$. Hence the Kutta condition that the vortex layer leaves the plate with zero gradient is satisfied; in particular $h^c(z) = O(z^{\frac{3}{2}})$ as $z \to 0^+$.

Thus the solution (5.7) satisfies all the boundary conditions. Also, it is causal and gives the correct Kutta condition.

## 6. The far field

The acoustic field of most interest is that experienced at large distances from the origin. This field can be determined asymptotically using the method of stationary phase.

The relevant causal solution is obtained when $k$ is real and positive, i.e. $\delta = 0$. For $\delta \to 0$ re-express $F_+(s)$ in terms of $\chi_+(s)$ and $\chi_-(s)$ by substituting $\hat{\mu}_+(s) = \chi_+(s)/(s - s_3)$ and $\hat{\mu}_-(s) = (s - s_0)\chi_-(s)$ into (5.3). Also, for convenience substitute $s = -iku$ into (5.7). The causal field in $r > a$ is then given by

$$\psi^c(r,z) = \lim_{\delta \to 0} \frac{1}{2\pi i} \int_{\infty \exp(i\delta)}^{-\infty \exp(i\delta)} \frac{K_3[1 - M\alpha u]\,[1 - u(1+M)]^{\frac{1}{2}}[C - u(1 + M\alpha C)]^{\frac{1}{2}}}{(u - u_0)\,(u - \mu/k)\,\chi_+(-iku)wH_n'^{(2)}(kaw)} \times H_n^{(2)}(kwr)\exp(-ikuz)\,du + G(k,r,z), \tag{6.1}$$

where the instability wave is

$$G(k,r,z) = \frac{K_3(1 - M\alpha u_0)\,[1 - u_0(1+M)]^{\frac{1}{2}}\,[C - u_0(1 + M\alpha C)]^{\frac{1}{2}} H_n'^{(2)}(krw_0)\exp(-iku_0 z)}{(u_0 - \mu/k)\,\chi_+(-iku_0)\,w_0\,H_n'^{(2)}(kaw_0)}, \tag{6.2}$$

$w_0$ is the value of $w$ at $u_0(k)$ and

$$K_3 = \frac{1}{2\pi}\left(1 - \frac{\mu}{k}M\right)\left(\frac{\mu}{k} - u_0\right)\chi_-(-i\mu)\left[1 + \frac{\mu}{k}(1 - M)\right]^{\frac{1}{2}}\left[C + \frac{\mu}{k}(1 - M\alpha C)\right]^{\frac{1}{2}}.$$

The contour of integration in (6.1) is the line $\mathrm{Im}\,(ku) = 0$, i.e. $C_1$. When $\delta = 0$ this contour $C_1$ collapses onto the real axis with small modifications to account for the branch points and poles. As shown in figure 3 ($a$) it passes below the branch cuts from $-\infty$ and above the branch cuts from $+\infty$. In general it can be taken to cross the real axis at $u = -M/(1 - M^2)$, passing below any poles near the real axis for which

$$\mathrm{Re}\,u < -M/(1 - M^2).$$

For possible exceptions to this rule the reader is referred to a paper by Morgan (1975).

Let

$$r = \rho(1 - M^2\alpha^2C^2)^{\frac{1}{2}}\sin\theta, \quad z = \rho(1 - M^2\alpha^2C^2)\cos\theta,$$

where $\rho > 0$ and $0 < \theta < \pi$. Now deform the contour $C_1$ into the curve

$$u = \frac{C\cos(\theta - i\tau) - M\alpha C^2}{1 - M^2\alpha^2C^2}, \tag{6.3}$$

which for large distances from the origin becomes the stationary-phase contour. Here $\tau$ is real with $-\infty < \tau < \infty$. The curve (6.3) is a branch of the hyperbola with asymptotes $u = e^{\pm i\theta}$ corresponding to $\tau = \pm\infty$, respectively.

The hyperbola avoids the branches provided that

$$-\sigma_2 < \frac{C\cos\theta - M\alpha C^2}{1-M^2\alpha^2C^2} < \sigma_1, \tag{6.4}$$

where $\sigma_1$ and $\sigma_2$ are defined by (2.12). When (6.4) is not satisfied the vertex of the hyperbola, given by $\tau = 0$, lies on the branch cut of $v$. This occurs if either

$$(a)\ \ \sigma_1 = 1/(1+M) \text{ and } \theta \text{ is small enough}$$

or

$$(b)\ \ \sigma_2 = 1/(1-M) \text{ and } \theta \text{ is large enough.}$$

In either case it is necessary to join the two points of the hyperbola corresponding to $\tau = 0\pm$ by a loop round the relevant branch point of $v$.

Assume for the moment that (6.4) holds. Let

$$u_0 = \frac{C\cos(\theta_0 - i\tau_0) - M\alpha C^2}{1-M^2\alpha^2C^2} = |u_0|\exp(i\beta_0),$$

where $\beta_0$, $\theta_0$ and $\tau_0$ are real and such that $0 < \beta_0 < \frac{1}{2}\pi$, $0 < \theta_0 < \frac{1}{2}\pi$ and $\tau_0 > 0$. Then for $k\rho \gg 1$, and when all poles except that at $u_0$ are ignored, we may write

$$\begin{aligned}\psi^c(r,z) = &-\frac{K_3}{2\pi}\int_{-\infty}^{\infty} \frac{(1-M\alpha u)[1-u(1+M)]^{\frac{1}{2}}[C-u(1+M\alpha C)]^{\frac{1}{2}}}{(u-u_0)(u-\mu/k)(1-M^2\alpha^2C^2)\chi_+(-iku)wH_n'^{(2)}(kaw)} \\ &\times\left[\frac{2C}{\pi k\rho}\frac{\sin(\theta-i\tau)}{\sin\theta}\right]^{\frac{1}{2}}\exp\{-ikC\cosh\tau + ik\rho M\alpha C^2\cos\theta + \tfrac{1}{2}n\pi i + \tfrac{1}{4}\pi i\}\,d\tau \\ &+ H(\theta_0-\theta)\,G(r,z),\end{aligned} \tag{6.5}$$

where $H(x)$ is the unit Heaviside function, which is zero if $x < 0$, $\frac{1}{2}$ if $x = 0$ and 1 for $x > 0$. The integral may now be evaluated asymptotically by the method of stationary phase. Thus, provided that $\theta$ is not near 0 or $\pi$, the field at large distances from the origin is

$$\begin{aligned}&\psi^c(r,z) \sim \\ &-\frac{K_3(1-M\alpha u)[1-u(1+M)]^{\frac{1}{2}}[C-u(1+M\alpha C)]^{\frac{1}{2}}\exp\{-ik\rho C(1-M\alpha C\cos\theta)+\frac{1}{2}n\pi i\}}{\pi k\rho(u-u_0)(u-\mu/k)(1-M^2\alpha^2C^2)\chi_+(-iku)wH_n'^{(2)}(kaw)} \\ &+ H(\theta_0-\theta)\,G(r,z),\end{aligned} \tag{6.6}$$

with $$u = C(\cos\theta - M\alpha C)/(1-M^2\alpha^2C^2).$$

In deriving (6.6) we have ignored all poles captured, with the exception of $u_0$, as the contour of integration is deformed into that of stationary phase. However the residue at $u = \mu/k$ is zero and for the other poles, associated with zeros of $\chi_+(-iku)$, it is easily deduced that the residue at each pole captured is exponentially damped. So the terms in (6.6) dominate each of these residues in the far field. The question arises as to whether the infinite sum of the residues is significant. This point is discussed by Morgan (1975) and one can extend the arguments to this problem to show that the sum is still insignificant when compared with the terms in (6.6).

When (6.4) is not satisfied there is an additional loop around the branch cut to investigate. Now $\chi(-iku)/vw$ has the same value on either side of the branch cut of $v$ for points lying on the cut but between the branch points of $w$. Therefore

$$\chi_+(-iku)[1-u(1+M)]^{-\frac{1}{2}}[C-u(1+M\alpha C)]^{-\frac{1}{2}}$$

also has the same value on the top and bottom edges of this portion of the branch cut. So the contribution from the loop round the branch cut is zero. The far field is therefore given by (6.6) for all $\theta$ not close to 0 or $\pi$.

## 7. Numerical calculations

In this section some numerical results for the far-field radiation pattern are discussed and comparisons are made with experimental work. The sound pressure

$$P(r,z) = -\rho_a c_a C(ik + M\alpha\partial/\partial z)\,\psi^c(r,z),$$

with $\psi^c$ given by expression (6.6), has been used in these calculations but, since the instability wave is difficult to portray in the far field, the term $H(\theta_0-\theta)\,G(r,z)$ has been ignored. The comparisons will therefore be of relevance in the region $\theta > \theta_0$, where $\theta_0 < 90°$. Flight simulation, for instance, decreases this angle $\theta_0$; e.g. $\theta_0 \to 0$ as $\alpha \to 1$. When $\theta < \theta_0$ the instability term dominates the far field and describes a sound wave that grows exponentially with distance downstream. Such growth cannot continue indefinitely since at some stage nonlinearities will become important. The physical mechanisms that are available to curtail the growth to the vortex layer have been discussed by Crow & Champagne (1971). Also a linear model has been proposed by Jones & Morgan (1974) and it may be possible to incorporate this in future work on the problem.

Let $r = R\sin\theta'$ and $z = R\cos\theta'$; then, omitting the $(\Theta, t)$ dependence, the sound pressure in the far field is

$$P(r,z) = \frac{\rho_a c_a Q(\theta')}{R} \exp\left\{\frac{ikRC}{1-M^2\alpha^2C^2}\left[M\alpha C\cos\theta' - (1-M^2\alpha^2C^2\sin^2\theta')^{\frac{1}{2}}\right] + \frac{(n+1)}{2}\pi i\right\},$$

where

$$Q(\theta') = \frac{CK_3(1-M\alpha u')^2[1-u'(1+M)]^{\frac{1}{2}}[C-u'(1+M\alpha C)]^{\frac{1}{2}}}{\pi H_n'^{(2)}(kaw')\,[1-M^2\alpha^2C^2\sin^2\theta']^{\frac{1}{2}}(u'-u_0)\,(u'-\mu/k)\,w'\chi_+(-iku')}.$$

Here

$$u' = \frac{C\cos\theta'\,[1-M^2\alpha^2C^2\sin^2\theta']^{-\frac{1}{2}} - M\alpha C^2}{1-M^2\alpha^2C^2}$$

$$w' = C\sin\theta'[1-M^2\alpha^2C^2\sin^2\theta']^{-\frac{1}{2}}.$$

Then the radiation pattern for the normalized sound pressure level can be written as

$$20\log_{10}\left|\frac{Q(\theta')}{[k(k^2-j_{n,m}'^2/a^2)^{\frac{1}{2}}]^{\frac{1}{2}}}\right| \text{ decibels}$$

and is presented in figures 6–15 for a variety of parameter values. In this the most difficult expressions to calculate are $|\chi_+(-iku')|$ and $|\chi_-(-i\mu)| = |\chi_+(-i\mu)/\chi(-i\mu)|$ since $I_1$ and $B_1$ in (4.8) and (4.10), respectively, need to be evaluated numerically.

In figures 6 and 7 we have presented the effect of external flow on the radiation pattern for the (0, 0) plane wave and the (0, 1) mode, respectively. Here the $(a, b)$ mode corresponds to $n = a$ and $m = b$. The results are given for a jet Mach number $M = 0{\cdot}5$, $ka = 4{\cdot}0$ and three values of $\alpha$ corresponding to no external flow ($\alpha = 0$), $\alpha = 0{\cdot}5$ and the case when the external flow velocity equals that of the jet ($\alpha = 1{\cdot}0$). In figure 6(*a*) we notice that when $\alpha = 0$ the noise level peaks at around 50° to the jet axis. As $\alpha$ increases, this angle, $\theta_p$ say, decreases until the peak is at 0° when $\alpha = 1$. The region of

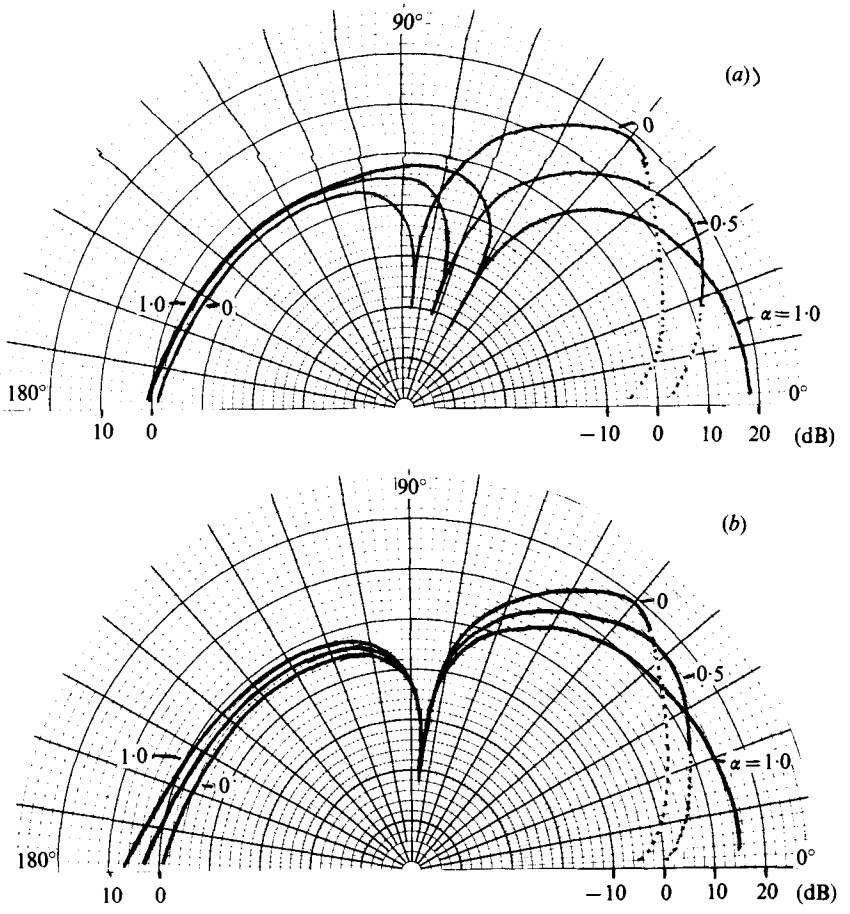


FIGURE 6. Radiation pattern for (0, 0) mode with flow mismatch ($\alpha$ varies), $M = 0{\cdot}5$, $ka = 4{\cdot}0$, $C = \gamma = 1{\cdot}0$. (*a*) 'Reception time' results. (*b*) 'Emission time' results. ····, region of influence for instability wave.

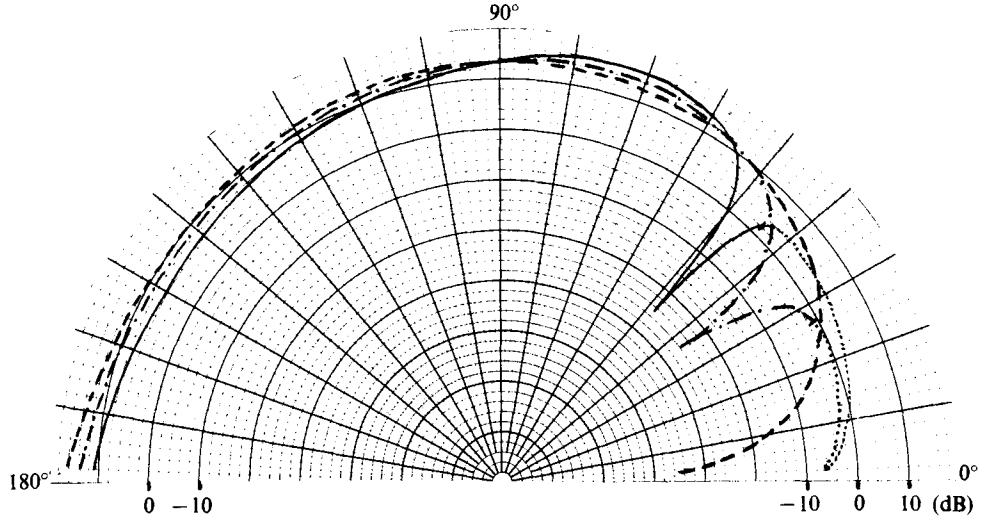


FIGURE 7. 'Emission time' radiation pattern for (0, 1) mode with varying $\alpha$; $M = 0{\cdot}5$, $ka = 4{\cdot}0$, $C = \gamma = 1{\cdot}0$. ——, $\alpha = 0$; —·—, $\alpha = 0{\cdot}5$; – – –, $\alpha = 1{\cdot}0$; ····, region of influence for instability wave.

influence of the instability wave is also indicated and depends on $\alpha$ in a similar way; i.e. $\theta_0$ decreases from 45° to 0° as $\alpha$ increases from 0 to 1. This instability wave, which is an inseparable part of the solution for $\theta < \theta_0$ but is not accounted for in the results, can be anticipated to dominate the relatively quiet region (the 'downstream zone of silence') that is noticeable close to the jet axis when $\alpha \neq 1$. Also, in the upstream direction ($\theta' \geqslant 90°$) it can be seen that the noise level increases with external flow and, for $ka = 4{\cdot}0$, is most noticeable at 90° to the jet axis. However these results pertain to observations in the 'reception time' co-ordinates $(R, \theta')$. To study the effects of flight it is usual to quote the results in 'emission time' co-ordinates $(r_e, \theta_e)$ which are related to $(R, \theta')$ through

$$\theta_e = \theta' + \sin^{-1}[M\alpha C \sin\theta']$$

and

$$r_e = R/\{1 + M\alpha C[M\alpha C + 2\cos\theta_e]\}^{\frac{1}{2}}.$$

The effects of flight in 'emission time' co-ordinates are presented in figure 6(*b*). In contrast to the 'reception time' results, we observe that the level at 90° is not significantly dependent on $\alpha$ and therefore on flight.† None of the other features, i.e. the increase in upstream level with $\alpha$ and the dependence of $\theta_p$ and $\theta_0$ on $\alpha$, are qualitatively altered by the co-ordinate transformation. For the (0, 1) mode the effect of the external flow on the 'emission time' radiation pattern, presented in figure 7, shows similar trends to those of the (0, 0) mode.

The result of varying the jet density and acoustic speed independently of each other is shown in figures 8 and 9, respectively, for a jet with no external flow ($\alpha = 0$). We observe in figure 8 that increasing the jet density, which corresponds to a decrease in $\gamma$, results in an increase in the noise level at all angles. For the variation of the acoustic speed, with $\gamma = 1$, we have illustrated two cases. In the first case, figure 9(*a*), the sound frequency is kept constant thus $ka$ varies with the acoustic speed. A general trend is difficult to extract in this case since the 'lobe' structure is highly dependent on $ka$. However a trend can be extracted in the second case, in which $ka$ is kept constant whilst the jet acoustic speed varies. This is shown in figure 9(*b*). It is then evident that the effect of increasing the jet acoustic speed, corresponding to an increase in $C$, is to beam the sound to the side. This feature has also been observed by Mani (1974) for a jet devoid of rigid boundaries. Also it should be noted that the angle $\theta_0$, which defines the region influenced by the instability wave, increases with $\gamma$ or $C$. Therefore when the jet is heated, which corresponds to an increase in $\gamma$ and $C$, we can expect a larger angular region of the radiation pattern to be influenced by the instability wave.

A number of calculations of the radiation pattern have also been presented by Savkar (1975), who used the Carrier–Koiter approximation for the same problem. A comparison with this work is given in figures 10–12. For the asymmetric (4, 1) mode the comparison, in figure 10, for the flow mismatch shows that there is an additional zero in the field for Savkar's calculation. This can be traced to when the stationary-phase point experiences the branch point $1/(1 + M)$. The differences can be shown to be a property of the Carrier–Koiter approximation by comparing Savkar's $L(\alpha)$ and $L^*(\alpha)$ at this point. In figure 11 the check is extended to include the experimental results of Plumblee & Dean (1973) for the (0, 0) mode. The agreement is not particularly good for either the present work or that of Savkar. However this is probably

† The author is indebted to a referee for indicating that in 'emission time' co-ordinates the level at 90° would not be affected by flight.

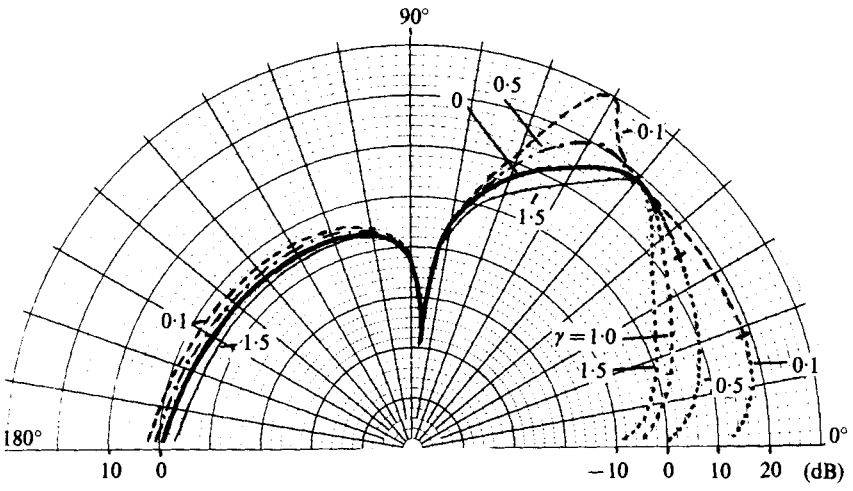


FIGURE 8. Radiation pattern for (0, 0) mode with density mismatch and no external flow; $\gamma$ varies, $\alpha = 0$, $M = 0{\cdot}5$, $ka = 4{\cdot}0$, $C = 1{\cdot}0$. · · · ·, region of influence for instability wave.

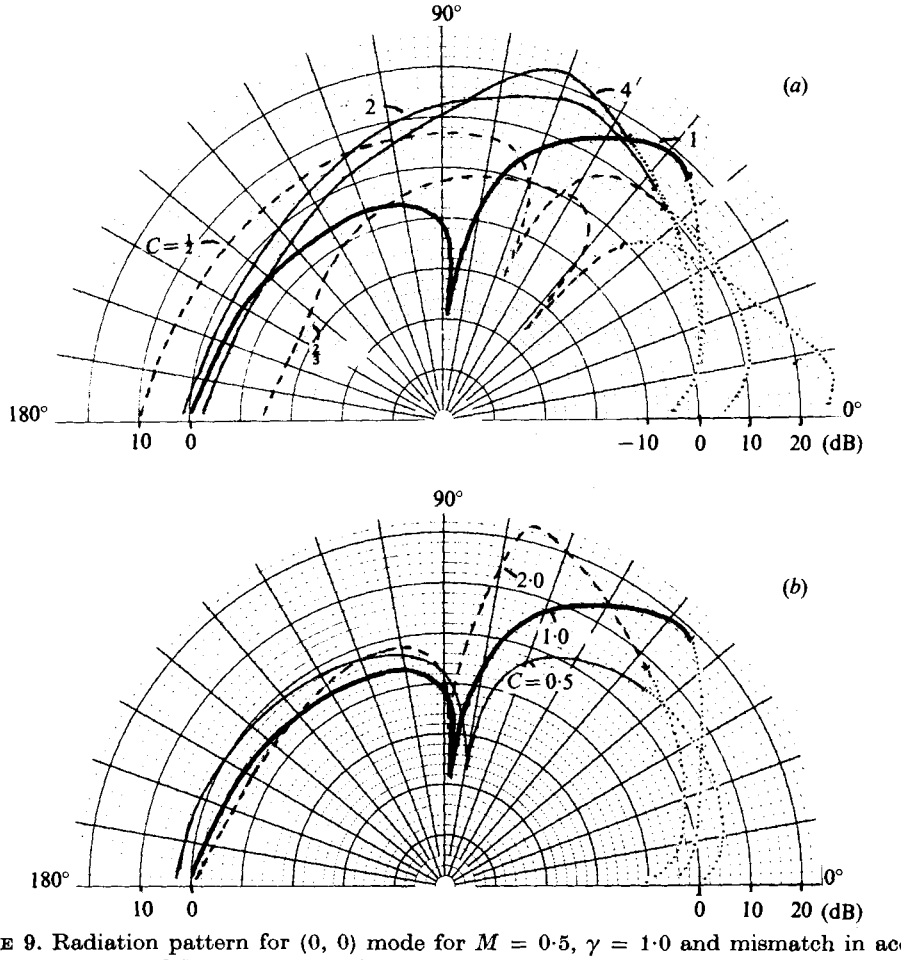


FIGURE 9. Radiation pattern for (0, 0) mode for $M = 0{\cdot}5$, $\gamma = 1{\cdot}0$ and mismatch in acoustic speed with no external flow ($\alpha = 0$). (*a*) Constant frequency, jet acoustic speed varies, $Cka = 4{\cdot}0$. (*b*) External acoustic speed varies, constant jet acoustic speed, $ka = 4{\cdot}0$. · · · · ·, region of influence for instability wave.

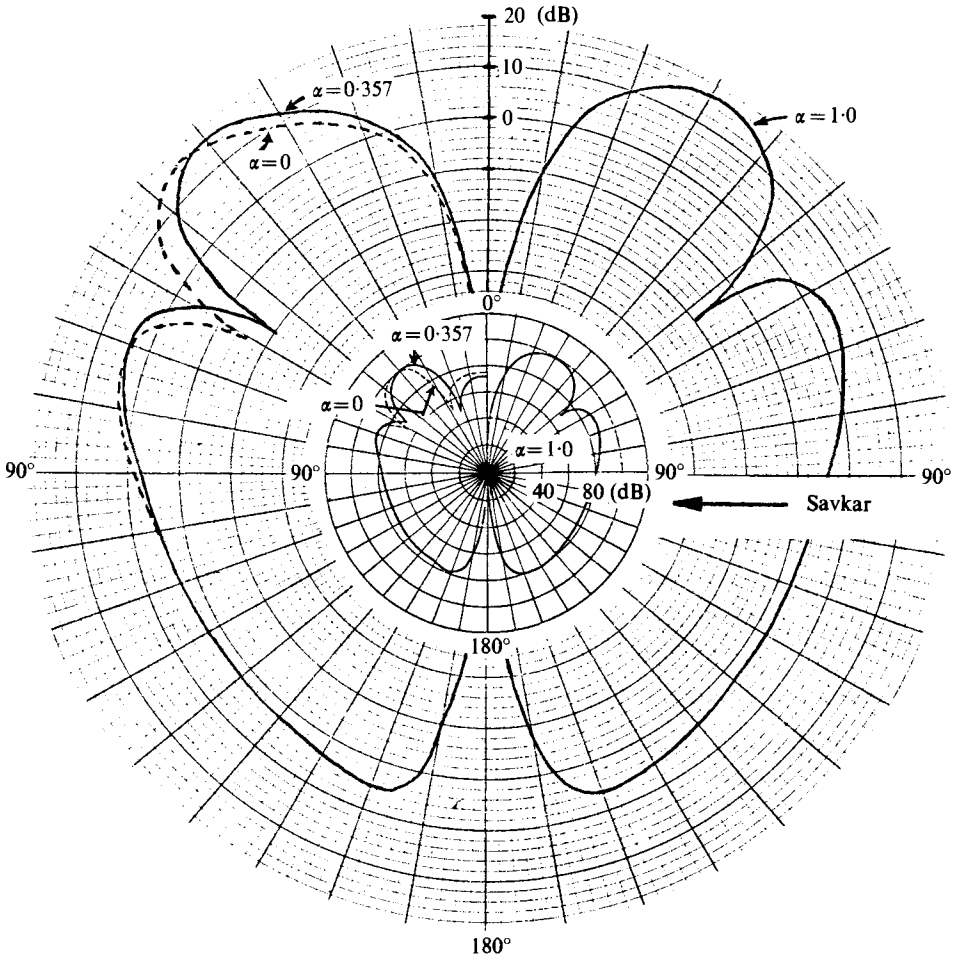


FIGURE 10. Comparison with Savkar (his figure 10) for (4, 1) mode, $ka = 11{\cdot}7$, $M = 0{\cdot}14$, $C = \gamma = 1{\cdot}0$.

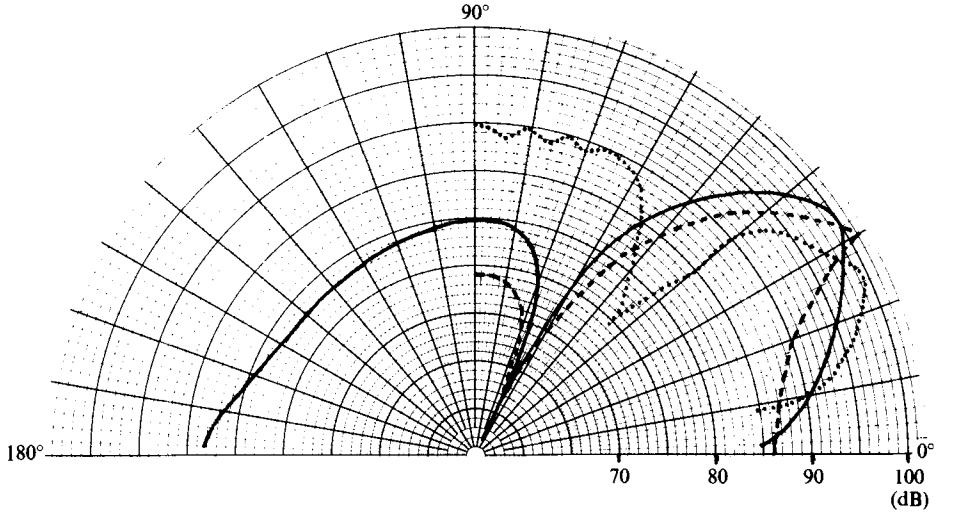


FIGURE 11. Comparison of theoretical (0, 0) radiation pattern (solid curves) with Carrier–Koiter approximation of Savkar (his figure 6, dashed curves) and data of Plumblee & Dean (dotted curves). Flow velocity = 150 ft/s, $M_j = 0{\cdot}134$, $\alpha = 0$, $ka = 4{\cdot}58$.

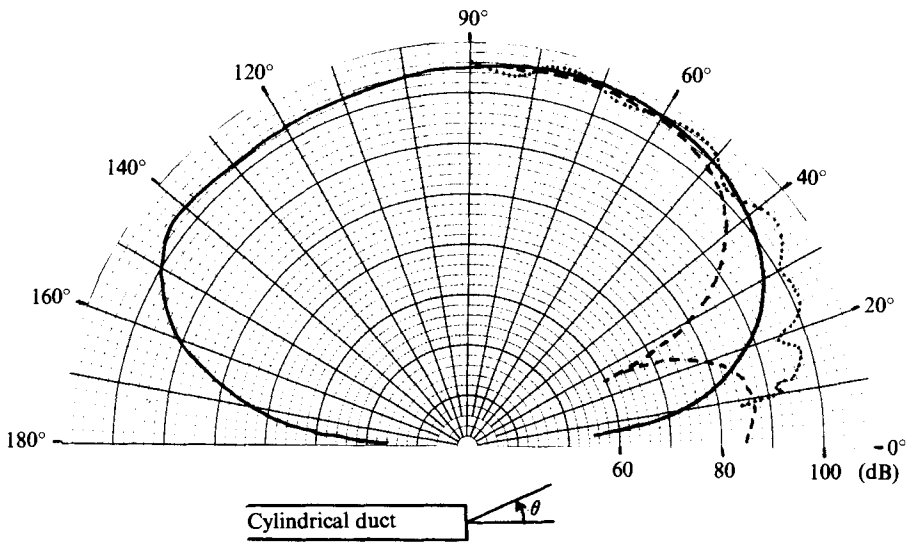


FIGURE 12. Comparison of theoretical (3, 1) radiation pattern (solid curves) with Carrier–Koiter approximation of Savkar (his figure 9, dashed curves) and data of Plumblee & Dean (their figure 19, dotted curves). Flow velocity = 150 ft/s, $M_j = 0{\cdot}134$, $\alpha = 0$, $ka = 4{\cdot}58$.

because Plumblee & Dean's experiment is for transmission of sound out of an annular duct, for which the modes of propagation depend on the roots of

$$J'_n(xa/b)\,Y'_n(x) - J'_n(x)\,Y'_n(xa/b) = 0$$

instead of $J'_n(x) = 0$. Specifically, the points of zero field will differ as shown in the figure. A further comparison is made in figure 12 for the (3, 1) mode and this shows better agreement with experiment. The point to make here is that the discrepancies in figure 12 for $\theta' < 40°$ could be an indication of the effect of instabilities although, as already pointed out, this could be a feature of the annular duct.

Experiments for which the present theory should be a relevant, although admittedly crude, model have been carried out recently by Pinker & Bryce (1976) and a comparison with their work is made in figures 13–15. In these experiments the frequency was restricted to a value below the cut-off frequency so that only the plane wave (0, 0) mode propagated. To simulate the effect of an infinite external flow (or 'flight') Pinker & Bryce immersed the jet in a second coaxial flow and applied the corrections of Jacques (1975) to the shear layer which separated this flow from still air. All the experimental measurements were carried out in the far-field, still-air region, within an anechoic chamber. Figures 13 and 14 compare the theoretical and experimental predictions for the radiation pattern for a cold jet. For the cases with no external flow the agreement between theory and experiment can be seen to be very good throughout the angular range considered in the experiments. Such agreement is surprising since the mathematical model does not take account of the effects of the contracting jet nozzle which is present in the experimental set up. Included in figure 13 is the comparison, in 'emission time' co-ordinates, for the far-field prediction in an external flow. Discrepancies in these 'flight' predictions at low angles to the jet axis may be due to the presence of the second shear layer in the experiments. Preliminary calculations for the problem

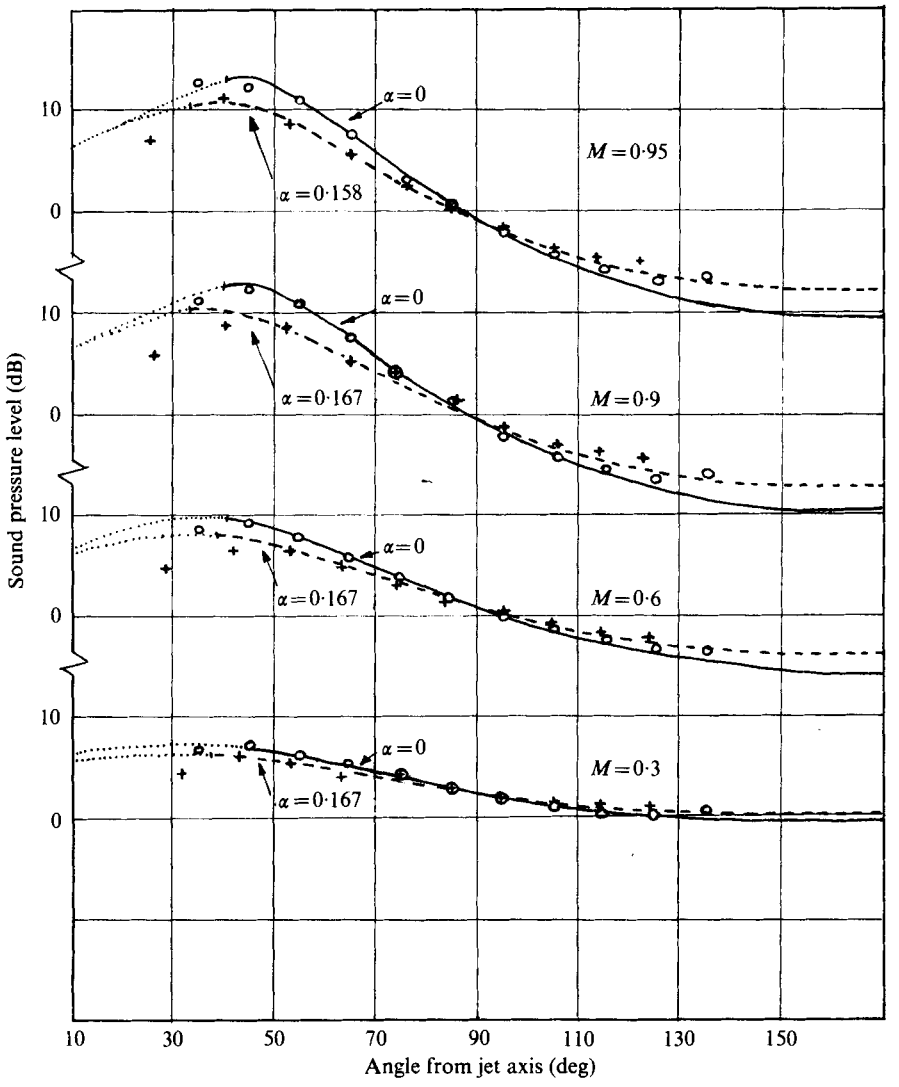


FIGURE 13. Comparison with experiment (Pinker & Bryce) for a cold jet ($C = \gamma = 1{\cdot}0$) at 2·5 kHz ($ka = 0{\cdot}6$) for the (0, 0) mode. Static jet ($\alpha = 0$): ——, theory; ○, experiment. Jet + external flow: – – –, theory; +, experiment. · · · ·, predicted region for instability wave. (Experiment matched with theory at 90° in static conditions.)

containing a secondary cylindrical vortex layer do indeed indicate better agreement with experiment at these low angles. However the details of this latter, more complicated problem will be left for another paper.

Comparisons with Pinker & Bryce for a hot jet with no external flow are given in figure 15. It appears that the jet density may be a critical factor. In particular, a curious fact is that the agreement with experiment improves on using $\gamma = 1$ instead of using the value derived from the conservation of static pressure across the vortex layer; i.e. $\gamma$ is given by $\gamma \simeq C^2$. However it should also be noted that the largest of the discrepancies occur in the region $\theta < \theta_0$ which is anticipated to be influenced by the

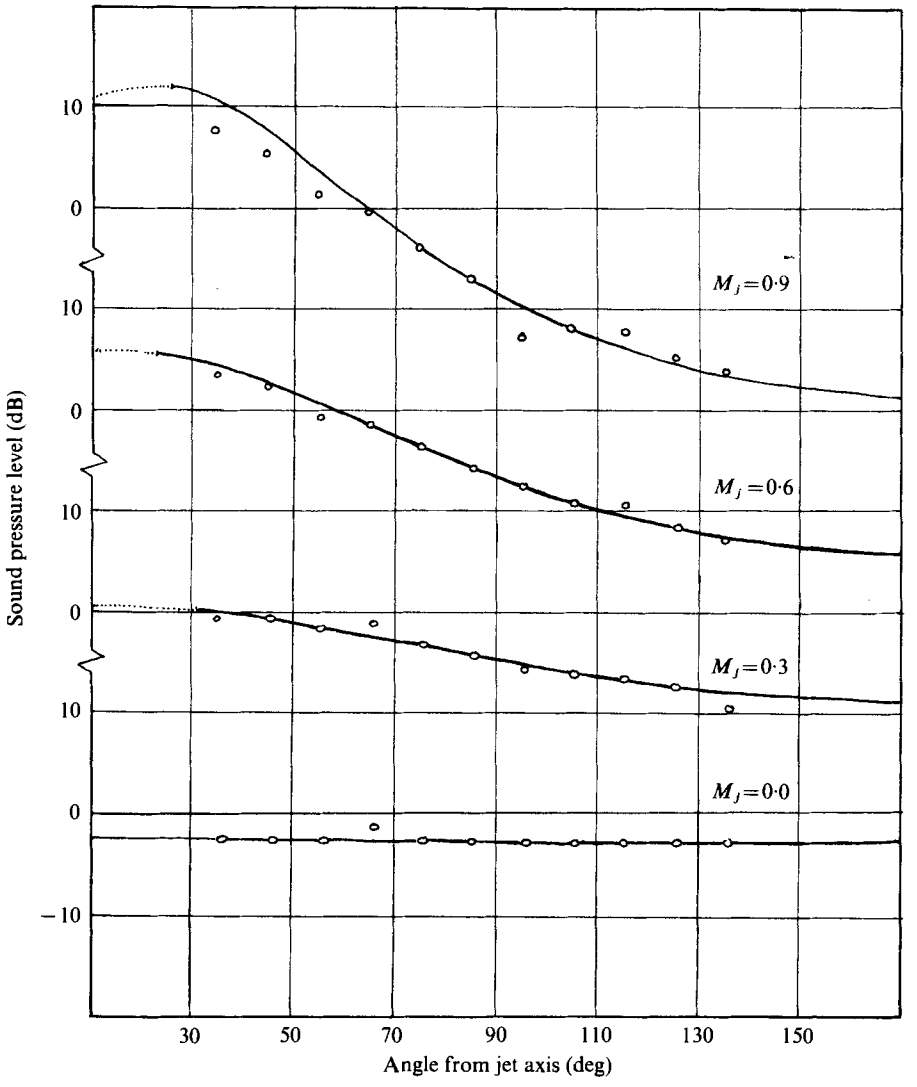


FIGURE 14. Comparison with experiment (Pinker & Bryce) for a cold jet at 1·0 kHz ($ka$ = 0·24) for the (0, 0) mode with $\alpha$ = 0. ——, theory; ○, experiment; · · · ·, predicted region for instability wave. (Experiment matched with theory at 90° in static conditions.)

instability wave. This would be consistent with a large contribution from the instability term $H(\theta_0-\theta)\,G(r,z)$ of (6.6), which we have not been able to include in the presentation of the results.

The author wishes to express his thanks to Professor D. S. Jones and Dr J. D. Morgan for many helpful discussions, specifically to J. D. Morgan for his computer algorithm to evaluate Bessel functions of complex argument. He would also like to thank the Science Research Council for the financial support to carry out the work.

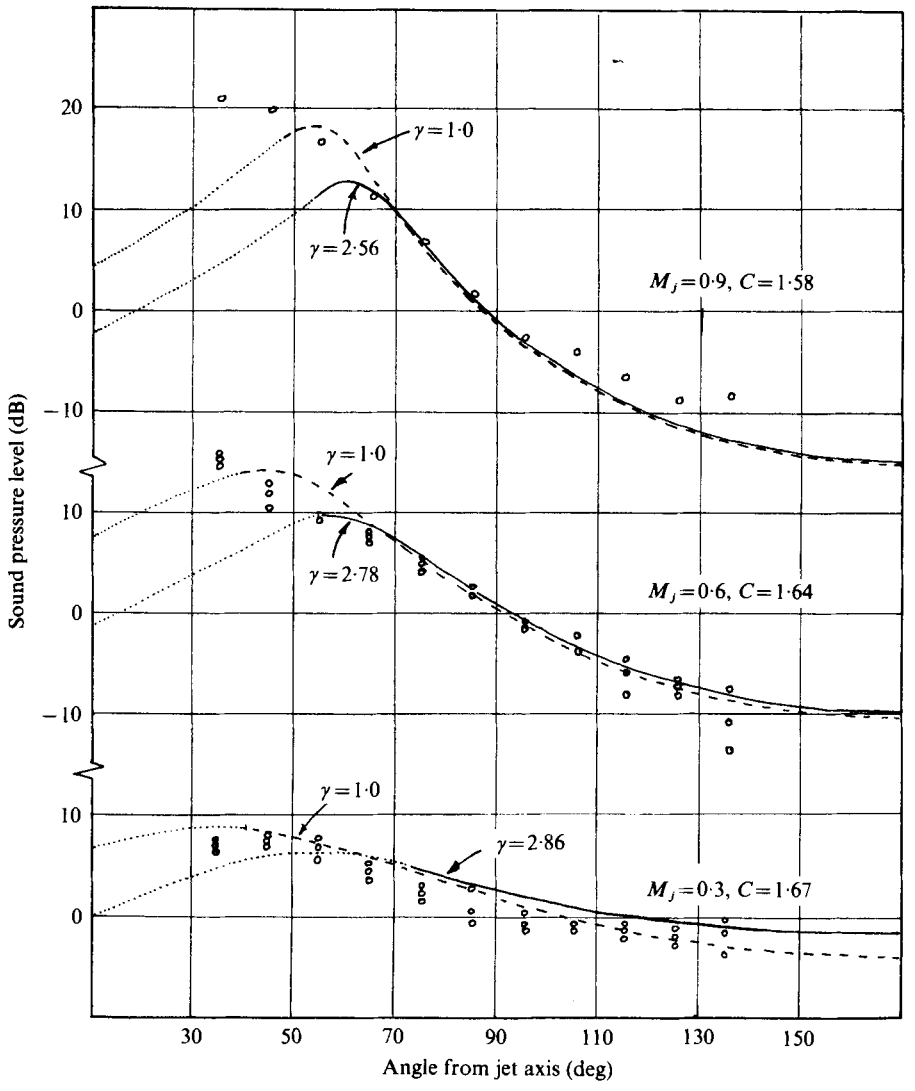


FIGURE 15. Comparison with experiment (Pinker & Bryce) for a hot static jet at 2·5 kHz $T_j$ = 830 °K and the (0, 0) mode. – – –, ——, theory; ○, experiment; · · · ·, predicted region for instability wave. (Experiment matched with theory at 90 ° in static conditions.)

## REFERENCES

BATCHELOR, G. K. & GILL, A. E. 1962 Analysis of the stability of axisymmetric jets. *J. Fluid Mech.* **14**, 529–551.

BECHERT, D. & PFIZENMAIER, E. 1975 Optical compensation measurements on the unsteady exit condition at a nozzle discharge edge. *J. Fluid Mech.* **71**, 123–144.

CANDEL, S. M. 1973 Acoustic radiation from the end of a two-dimensional duct, effects of uniform flow and duct lining. *J. Sound Vib.* **28**, 1–13. *Quart. Appl. Math.* **13**, 457–461.

CARRIER, G. F. 1956 Sound transmission from a tube with flow.

CHAN, Y. Y. & WESTLEY, R. 1973 Directional acoustic radiation generated by spatial jet instability. *C.A.S.I. Trans.* **6**, 36–41.

CRIGHTON, D. G. 1972*a* Radiation properties of the semi-infinite vortex sheet. *Proc. Roy. Soc.* A **330**, 185.

CRIGHTON, D. G. 1972*b* The excess noise field of subsonic jets. *J. Fluid Mech.* **56**, 683–694.

CRIGHTON, D. G. & LEPPINGTON, F. G. 1974 Radiation properties of the semi-infinite vortex sheet: the initial-value problem. *J. Fluid Mech.* **64**, 393–414.

CROW, S. C. 1972 Acoustic gain of a turbulent jet. *Am. Phys. Soc. Meeting, Boulder, Colorado*, paper IE.6.

CROW, S. C. & CHAMPAGNE, F. H. 1971 Orderly structure in jet turbulence. *J. Fluid Mech.* **48**, 547–591.

HARDISTY, N. 1975 The instability of two vortex sheets enclosing a subsonic jet due to an acoustic point source. *Proc. Roy. Soc. Edin.* A **73**, 215–229.

HOMICZ, G. F. & LORDI, J. A. 1975 A note on the radiative directivity patterns of duct acoustic modes. *J. Sound Vib.* **41**, 283–290.

HOWE, M. S. 1976 The influence of vortex shedding on the generation of sound by convected turbulence. *J. Fluid Mech.* **76**, 711–740.

JACQUES, J. R. 1975 The noise from moving aircraft; some relevant models. Ph.D. thesis, Cambridge University.

JONES, D. S. 1973 The convolution of generalised functions. *Quart. J. Math.* **24**, 145–163.

JONES, D. S. 1977 The scattering of sound by a simple shear layer. *Phil. Trans. Roy. Soc.* A **284**, 287–328.

JONES, D. S. & MORGAN, J. D. 1972 The instability of a vortex sheet on a subsonic stream under acoustic radiation. *Proc. Camb. Phil. Soc.* **72**, 465–488.

JONES, D. S. & MORGAN, J. D. 1974 A linear model of a finite Helmholtz instability. *Proc. Roy. Soc.* A **338**, 17–41.

LANSING, D. L., DRISCHLER, J. A. & PUSEY, C. G. 1970 Radiation of sound from an unflanged circular duct with flow. *79th Meeting Acoust. Soc. Am.*

LEE, B. H. K. & JONES, D. J. 1973 Transmission of upstream sound through a subsonic jet. *A.I.A.A. Paper* no. 73-630.

MANI, R. 1973 Refraction of acoustic duct waveguide modes by exhaust jets. *Quart. Appl. Math.* **30**, 501–520.

MANI, R. 1974 The jet density exponent issue for the noise of heated subsonic jets. *J. Fluid Mech.* **64**, 611–622.

MORGAN, J. D. 1974 The interaction of sound with a semi-infinite vortex sheet. *Quart. J. Mech. Appl. Math.* **27**, 465–487.

MORGAN, J. D. 1975 The interaction of sound with a subsonic cylindrical vortex sheet. *Proc. Roy. Soc.* A **344**, 341–362.

MUNT, R. M. 1975 Acoustic radiation from a circular cylinder in a subsonic stream. *J. Inst. Math.* **16**, 1–10.

NOBLE, B. 1958 *Methods based on the Wiener–Hopf Technique.* Pergamon.

ORSZAG, S. A. & CROW, S. C. 1970 Instability of a vortex sheet leaving a semi-infinite plate. *Stud. Appl. Math.* **49**, 167–181.

PINKER, R. A. & BRYCE, W. D. 1976 The radiation of plane wave duct noise from a jet exhaust, statically and in flight. *A.I.A.A. Paper* no. 76-581.

PLUMBLEE, H. E. & DEAN, P. D. 1973 Sound measurements within and in the radiated field of an annular duct with flow. *J. Sound Vib.* **28**, 715–735.

SAVKAR, S. D. 1975 Radiation of cylindrical duct acoustic modes with flow mismatch. *J. Sound Vib.* **42**, 363–386.

TAM, C. K. W. 1971 Directional acoustic radiation from a supersonic jet generated by a shear layer instability. *J. Fluid Mech.* **46**, 757–768.

WATSON, G. N. 1966 *Theory of Bessel Functions.* Cambridge University Press.